

NUMERICAL ANALYSIS OF THE CAUSAL ACTION PRINCIPLE IN LOW DIMENSIONS

FELIX FINSTER, ROBERT H. JONSSON, AND NIKI KILBERTUS

JANUARY 2022

ABSTRACT. The numerical analysis of causal fermion systems is advanced by employing differentiable programming methods. The causal action principle for weighted counting measures is introduced for general values of the integer parameters f (the particle number), n (the spin dimension) and m (the number of spacetime points). In the case $n = 1$, the causal relations are clarified geometrically in terms of causal cones. Discrete Dirac spheres are introduced as candidates for minimizers for large m in the cases $n = 1, f = 2$ and $n = 2, f = 4$. We provide a thorough numerical analysis of the causal action principle for weighted counting measures for large m in the cases $n = 1, 2$ and $f = 2, 3, 4$. Our numerical findings corroborate that all minimizers for large m are good approximations of the discrete Dirac spheres. In the example $n = 1, f = 3$ it is explained how numerical minimizers can be visualized by projected spacetime plots. Methods and prospects are discussed to numerically investigate settings in which hitherto no analytic candidates for minimizers are known.

CONTENTS

1. Introduction	2
2. The Causal Action Principle for Weighted Counting Measures	3
3. The Causal Action Principle on a Two-Dimensional Hilbert Space	5
3.1. The Lagrangian and the Causal Structure	6
3.2. Qualitative Description of Underlying Mechanisms	8
3.3. Minimizing in the Class of Isotropic Measures	9
3.4. The Two-Dimensional Discrete Dirac Sphere	11
3.5. Causally Trivial Measures as Local Minimizers	13
4. The Four-Dimensional Discrete Dirac Sphere	15
5. Causal Cones in Spin Dimension One	20
6. Numerical Analysis	22
6.1. Overview and Optimization Choices	22
6.2. Parametrization of the Optimization Problem	24
6.3. Initialization	25
7. The Asymptotics for Fixed m and Large f	25
7.1. Analytic Results	25
7.2. Numerical Findings	28
8. Numerical Study of Discrete Dirac Spheres	29
8.1. Spin Dimension One	29
8.2. Spin Dimension Two	31
9. Numerical Study beyond Discrete Dirac Spheres	31
10. Conclusion and Outlook	34

Appendix A. Details of the Implementation	34
References	36

1. INTRODUCTION

The theory of *causal fermion systems* is a recent approach to fundamental physics (see the reviews [17, 14, 13], the textbook [12] or the website [1]). In this approach, spacetime and all objects therein are described by a measure ρ on a set \mathcal{F} of linear operators of a Hilbert space $(\mathcal{H}, \langle \cdot | \cdot \rangle_{\mathcal{H}})$. The physical equations are formulated via the so-called *causal action principle*, a nonlinear variational principle where an action \mathcal{S} is minimized under variations of the measure ρ .

While the causal action principle has been analyzed in detail from an abstract point of view, only very few examples of exact minimizers are known. In [9, 19, 5] a few simple minimizers were constructed numerically in low dimensions and for a small number of spacetime points. Moreover, the Dirac sea vacuum used as the starting point for most applications is known to be a minimizer, but only in a specific limiting case when the ultraviolet regularization is removed (for details see [12, Chapters 3-5]). In view of the lack of explicit examples, it is an important task to minimize the causal action numerically for many spacetime points and, eventually, in a high-dimensional Hilbert space, with the goal of clarifying the structure of the minimizing measures. The present paper is a first step towards this goal, where we consider Hilbert spaces of low dimension two, three and four.

In the causal action principle, one minimizes the causal action under variations of a measure ρ within the class of all regular Borel measures, under three constraints: the volume, the trace and the boundedness constraints. In order to describe the measure numerically, we here restrict our attention to *weighted counting measures* ρ of the form

$$\rho = \sum_{i=1}^m c_i \delta_{x_i},$$

where δ_{x_i} is the Dirac measure supported at $x_i \in \mathcal{F}$, and the coefficients c_i are non-negative weight factors. Choosing m large enough, one can approximate any regular Borel measure by such weighted counting measures. Clearly, in the numerical study one needs to choose m finite. But information on general minimizing measures can be obtained by considering the asymptotics for large m . The volume and trace constraints can be implemented by considering *normalized* measures on operators of *fixed trace*, i.e.

$$\sum_{i=1}^m c_i = 1 \quad \text{and} \quad \text{tr } x_i = 1 \text{ for all } i = 1, \dots, m.$$

The boundedness constraint, on the other hand, is needed in order to ensure that the points x_i remain bounded and the infimum of the causal action remains strictly positive in the limit $m \rightarrow \infty$. Since m will be fixed when minimizing numerically, here we may leave out the boundedness constraint. Instead, the necessity of the boundedness constraint will become apparent in the fact that the causal action found numerically in the case $n = 2$ will tend to zero asymptotically for large m .

Minimizing the causal action principle can be regarded as a problem of nonlinear optimization. The number of parameters grows linearly in the dimension f of the

Hilbert space. Therefore, the numerical analysis becomes more difficult the larger the dimension f of the Hilbert space is chosen. For this reason, we here focus on the low-dimensional cases

$$f = 2, 3 \text{ and } 4,$$

with the main goal of analyzing the asymptotics for large m . In the cases $n = 1, f = 2$ and $n = 2, f = 4$ it is conjectured that, asymptotically for large m , the minimizing measures should have the form of equally spaced points on a sphere of dimension two (if $f = 2$) or four (if $f = 4$), where the radius of the sphere tends to infinity for large m . These so-called *discrete Dirac sphere configurations* will be introduced in detail in Sections 3.4 and 4. Our numerical results support the conjecture that such discrete Dirac sphere configurations are indeed the only minimizing measures for large m .

Our numerical findings also triggered a more detailed analytic study, which gave some new insight into the structure of the causal action principle. These analytic results will also be derived and explained in the present paper. In particular, we realized that, in the case of spin dimension $n = 1$, the causal relations on \mathcal{F} gives rise to cones. This is worked out in Sections 3.1 and 5 (see also Figure 1 on page 8 and Figure 2 on page 22). Moreover, the asymptotics for fixed m and large f was worked out and compared to the numerical findings (see Section 7).

Our numerical investigations also include the case $n = 1$ and $f = 3$. In this case, it is unknown how the minimizing measures should look like for large m . Therefore, our numerical approach can give new insight into the structure of minimizing measures in this setting and inspire progress regarding analytical results. To this end, in Section 9, we introduce *projected spacetime plots* as a tool to visualize the geometry and causal structure of a discrete spacetime, as seen from a reference spacetime point.

The paper is structured as follows. Section 2 provides the necessary background on causal fermion systems and the causal action principle. Section 3 is devoted to the case $f = 2$. After working out the Lagrangian and the causal structure in detail (Section 3.1), we explain the underlying mechanism qualitatively (Section 3.2). We proceed by computing the causal action for spherically symmetric measures (so-called isotropic measures; see Section 3.3). Then we show that the causal action can be decreased further by choosing discrete points on a sphere (the so-called discrete Dirac sphere; see Section 3.4). In these examples, the causal structure is trivial in the sense that all distinct spacetime points are spacelike separated. Such measures are analyzed in some more detail (Section 3.5). In Section 4 we turn our attention to the case $n = 2, f = 4$ and generalize the discrete Dirac sphere to this case. In Section 5 the considerations on the causal structure from Section 3.1 are generalized to a general dimension f of the Hilbert space. In Section 6 it is explained how we set up the problem numerically. Section 7 is devoted to the asymptotics for large f keeping m fixed. In Section 8 the cases $n = 1, f = 2$ and $n = 2, f = 4$ are investigated numerically. The numerical minimizers are compared to the discrete Dirac sphere configurations. In Section 9 we take the example $n = 1, f = 3$ to discuss prospects for numerical studies in the case $f > 2n$. In Section 10 we conclude the paper with a brief summary and outlook. Appendix A provides some details of our numerical implementation.

2. THE CAUSAL ACTION PRINCIPLE FOR WEIGHTED COUNTING MEASURES

For clarity, we first introduce the causal action principle for weighted counting measures and explain afterward the connection to the general causal action principle as

introduced in [12, §1.1.1]. For a more detailed introduction to the physical concepts and the mathematical structures we refer to the textbooks [12, 16].

Given a complex Hilbert space of finite dimension f and a parameter $n \in \mathbb{N}$ (the “spin dimension”), we let $\mathcal{F} \subset L(\mathcal{H})$ be the set of all symmetric¹ linear operators x on \mathcal{H} with trace one,

$$\operatorname{tr} x = 1, \quad (2.1)$$

which (counting multiplicities) have at most n positive and at most n negative eigenvalues. Next, we let ρ be a *normalized weighted counting measure* on \mathcal{F} (as first considered in the context of causal fermion systems in [19, Section 2]). Thus, given $m \in \mathbb{N}$, we choose points $x_1, \dots, x_m \in \mathcal{F}$ and corresponding weights c_1, \dots, c_m with

$$c_i \geq 0 \quad \text{and} \quad \sum_{i=1}^m c_i = 1. \quad (2.2)$$

We introduce the measure ρ by defining its integral of a continuous function f by

$$\int_{\mathcal{F}} f d\rho := \sum_{i=1}^m c_i f(x_i) \quad \text{for all } f \in C^0(\mathcal{F}). \quad (2.3)$$

We also use the shorter notation

$$\rho = \sum_{i=1}^m c_i \delta_{x_i}, \quad (2.4)$$

where δ_{x_i} is the Dirac measure supported at x_i .

For any $x, y \in \mathcal{F}$, the product xy is an operator of rank at most $2n$. We denote its non-trivial eigenvalues counting algebraic multiplicities by $\lambda_1^{xy}, \dots, \lambda_{2n}^{xy} \in \mathbb{C}$ (more specifically, denoting the rank of xy by $k \leq 2n$, we choose $\lambda_1^{xy}, \dots, \lambda_k^{xy}$ as all the non-zero eigenvalues and set $\lambda_{k+1}^{xy}, \dots, \lambda_{2n}^{xy} = 0$). We introduce the causal Lagrangian and the causal action by

$$\text{causal Lagrangian:} \quad \mathcal{L}(x, y) = \frac{1}{4n} \sum_{i,j=1}^{2n} \left(|\lambda_i^{xy}| - |\lambda_j^{xy}| \right)^2 \quad (2.5)$$

$$\text{causal action:} \quad \mathcal{S}(\rho) = \iint_{\mathcal{F} \times \mathcal{F}} \mathcal{L}(x, y) d\rho(x) d\rho(y). \quad (2.6)$$

The *causal action principle* is to minimize \mathcal{S} by varying ρ in the class of normalized weighted counting measures (2.3). The parameters entering this variational principle are

$$\begin{cases} n & \text{spin dimension} \\ m & \text{maximal number of points of weighted counting measure} \\ f & \text{dimension of the Hilbert space.} \end{cases}$$

The spectral properties of the operator product xy gives rise to the following *causal structure*. Two points $x, y \in \mathcal{F}$ are called *spacelike* separated if all the eigenvalues λ_j^{xy} have the same absolute value. They are said to be *timelike* separated if the λ_j^{xy} are all real and do not all have the same absolute value. In all other cases (i.e. if the λ_j^{xy} are not all real and do not all have the same absolute value), the points x and y are said

¹Here by a symmetric operator A we mean that $\langle Au|v \rangle_{\mathcal{H}} = \langle u|Av \rangle_{\mathcal{H}}$ for all $u, v \in \mathcal{H}$. Representing the operator in an orthonormal basis, the resulting matrix is Hermitian. For bounded operators as considered here, the notions “symmetric” and “selfadjoint” coincide.

to be *lightlike* separated. Evaluating these relations for the points x_1, \dots, x_m , we get corresponding causal relations between these points, which thus form our *spacetime* M ,

$$M := \{x_1, \dots, x_m\} \subset \mathcal{F}. \quad (2.7)$$

The causal action principle is compatible with the above causal structure in the following sense. Suppose that two spacetime points $x, y \in M$ are spacelike separated. Then the eigenvalues λ_i^{xy} all have the same absolute value, implying that the Lagrangian (2.5) vanishes. Working out the corresponding Euler-Lagrange equations (for details see [18] or [16, Chapter 7]), one finds that pairs of points with spacelike separation again drop out. This can be seen in analogy to the usual notion of causality where points with spacelike separation cannot influence each other. In this sense, the principle of causality is built into the theory of causal fermion systems.

We conclude by explaining how the above variational principle is obtained from the general causal action principle introduced in [12, §1.1.1]. Before beginning, we point out that, in order to allow for a numerical treatment, we clearly need to assume that \mathcal{H} is finite-dimensional and that ρ is a weighted counting measure. Moreover, using the rescaling freedom $\rho \rightarrow \sigma\rho$, it is no loss of generality to restrict attention to normalized measures. Next, using that minimizing measures are supported on operators of constant trace (see [12, Proposition 1.4.1]), we may fix the trace of the operators. Moreover, by rescaling the operators according to $x \rightarrow \lambda x$ with $\lambda \in \mathbb{R}$, one can assume without loss of generality that this trace is equal to one (2.1). Finally, as already mentioned in the introduction, we here disregard the so-called *boundedness constraint*, which states that all the measures ρ taken into account in the minimization process should satisfy the inequality

$$\mathcal{T}(\rho) := \iint_{\mathcal{F} \times \mathcal{F}} \left(\sum_{i=1}^{2n} |\lambda_i^{xy}| \right)^2 d\rho(x) d\rho(y) \leq C \quad (2.8)$$

for a given parameter $C > 0$. The boundedness constraint is needed for the causal action principle to be well-posed when varying within the class of all regular Borel measures. Specifically, in that case, it ensures compactness. However, in our setting of weighted counting measures with an upper bound m on the number of spacetime points, the boundedness constraint is *not needed* for the causal action principle to be well-posed. Nevertheless, the functional \mathcal{T} will be relevant for us when analyzing the asymptotics as $m \rightarrow \infty$. Indeed, in this limiting case, the support of the minimizing measures will typically tend to infinity. Likewise, the functional \mathcal{T} will tend to infinity. This phenomenon will be discussed in more detail at the end of Section 3.4 and in Section 4.

3. THE CAUSAL ACTION PRINCIPLE ON A TWO-DIMENSIONAL HILBERT SPACE

The simplest interesting setting of the causal action principle is to choose $n = 1$ and $f = 2$. In this section we analyze this case in detail. This will lead us to the conjecture that, for large values of m , minimizing measures should be close to so-called discrete Dirac sphere configurations (as will be introduced in Section 3.4). This section also sets the stage for the numerical analysis in Section 6, in which this conjecture will be examined.

We identify \mathcal{H} with $(\mathbb{C}^2, \langle \cdot, \cdot \rangle_{\mathbb{C}^2})$ (where $\langle \cdot, \cdot \rangle_{\mathbb{C}^2}$ denotes the standard Euclidean scalar product). Then the symmetric operators on \mathcal{H} are identified with the Hermitian 2×2 -matrices. Every such matrix can be represented as a real linear combination of the

identity matrix and the three Pauli matrices

$$\sigma^1 = \begin{pmatrix} 0 & 1 \\ 1 & 0 \end{pmatrix}, \quad \sigma^2 = \begin{pmatrix} 0 & -i \\ i & 0 \end{pmatrix} \quad \text{and} \quad \sigma^3 = \begin{pmatrix} 1 & 0 \\ 0 & -1 \end{pmatrix}. \quad (3.1)$$

Prescribing the trace (2.1) and imposing that the matrix should have at most one positive and at most one negative eigenvalue, one readily finds that the operators in \mathcal{F} can be identified with the complement of the open ball in \mathbb{R}^3 via the mapping

$$F : [1, \infty) \times S^2 \rightarrow \mathcal{F}, \quad (\tau, \vec{x}) \mapsto F_\tau(\vec{x}) = \frac{1}{2} \left(\mathbf{1} + \tau \sum_{i=1}^3 x^i \sigma^i \right) := \frac{1}{2} (\mathbf{1} + \tau \vec{x} \cdot \vec{\sigma}) \quad (3.2)$$

(here S^2 denotes the unit sphere in \mathbb{R}^3). Indeed, the matrix $F_\tau(\vec{x})$ clearly is Hermitian and has trace one. Conversely, every Hermitian matrix of trace one is the unique image of some $(\tau, \vec{x}) \in (1, \infty) \times S^2$. Next, the matrix $F_\tau(\vec{x})$ satisfies the polynomial equation

$$(2F_\tau(\vec{x}) - \mathbf{1})^2 = \left(\sum_{i=1}^3 \tau x^i \sigma^i \right)^2 = \tau^2 \mathbf{1},$$

where in the last step we used the anti-commutation relations for Pauli matrices $\{\sigma^i, \sigma^j\} = 2\delta^{ij}$. Consequently, the eigenvalues of $F_\tau(\vec{x})$ are given by

$$\nu_\pm = \frac{1}{2} (1 \pm \tau). \quad (3.3)$$

In particular, as desired, $F_\tau(\vec{x})$ has at most one positive and at most one negative eigenvalue.

To simplify notation, in what follows we use the map F in (3.2) to identify \mathcal{F} with the set $[1, \infty) \times S^2$. We also write $F_\tau(\vec{x})$ simply as $(\tau, \vec{x}) \in \mathcal{F}$.

3.1. The Lagrangian and the Causal Structure. Before analyzing the causal action principle, we need to compute the Lagrangian for two general arguments in \mathcal{F} .

Lemma 3.1. *Let $\tau, \tau' \in [1, \infty)$ and $\vec{x}, \vec{x}' \in S^2$. We denote the angle between \vec{x} and \vec{x}' by $\vartheta \in [0, \pi]$ (i.e. $\cos \vartheta = \vec{x} \cdot \vec{x}'$). Then the operator product $F_\tau(\vec{x})F_{\tau'}(\vec{x}')$ has the eigenvalues*

$$\lambda_{1,2} = \frac{1}{4} \left(1 + \tau\tau' \cos \vartheta \pm \sqrt{(1 + \tau\tau' \cos \vartheta)^2 - (\tau^2 - 1)(\tau'^2 - 1)} \right). \quad (3.4)$$

Moreover,

$$\mathcal{L}((\tau, \vec{x}), (\tau', \vec{x}')) = \frac{1}{8} \left((1 + \tau\tau' \cos \vartheta)^2 - (\tau^2 - 1)(\tau'^2 - 1) \right) (1 - \chi_{[\vartheta_-, \vartheta_+]}(\vartheta)), \quad (3.5)$$

where $\chi_{[\vartheta_-, \vartheta_+]}$ is the characteristic function of the interval defined by

$$\cos \vartheta_\pm = \frac{-1 \mp \sqrt{(\tau^2 - 1)(\tau'^2 - 1)}}{\tau\tau'}. \quad (3.6)$$

Proof. The proof is a direct generalization of the computations in the case $\tau = \tau'$ as carried out in [9, Proposition 4.1] and [11, Example 2.8]. Using the identity between Pauli matrices

$$\sigma^j \sigma^k = \delta^{jk} \mathbf{1} + i \epsilon^{jkl} \sigma^l$$

(where ϵ^{jkl} is the totally anti-symmetric Levi-Civita symbol), one obtains

$$F_\tau(\vec{x}) F_{\tau'}(\vec{x}') = \frac{1}{4} \left((\tau\tau' \cos \vartheta + 1) \mathbf{1} + (\tau \vec{x} + \tau' \vec{x}' + i\tau\tau' \vec{x} \wedge \vec{x}') \cdot \vec{\sigma} \right) \quad (3.7)$$

(where the wedge product is defined by $(\vec{x} \wedge \vec{y})^l = \epsilon^{jkl} x^j y^k$). Using that the vector $\vec{x} \wedge \vec{x}'$ is orthogonal to both \vec{x} and \vec{x}' , a direct computation using the transformation

$$\tau^2 + \tau'^2 + 2\tau\tau' \cos \vartheta - \tau^2 \tau'^2 \sin^2 \vartheta = (1 + \tau\tau' \cos \vartheta)^2 - (\tau^2 - 1)(\tau'^2 - 1)$$

shows that

$$\left(F_\tau(\vec{x}) F_{\tau'}(\vec{x}') - \frac{1}{4} (\tau\tau' \cos \vartheta + 1) \mathbb{1} \right)^2 = \frac{1}{16} \left((1 + \tau\tau' \cos \vartheta)^2 - (\tau^2 - 1)(\tau'^2 - 1) \right) \mathbb{1}.$$

The eigenvalues of $F_\tau(\vec{x}) F_{\tau'}(\vec{x}')$ are the roots of this polynomial. This gives (3.4).

If the vectors \vec{x} and \vec{x}' are collinear, these eigenvalues simplify to

$$\lambda_{1,2} = \begin{cases} \frac{1}{4} (1 \pm \tau)(1 \pm \tau') > 0 & \text{if } \vartheta = 0 \\ \frac{1}{4} (1 \pm \tau)(1 \mp \tau') < 0 & \text{if } \vartheta = \pi. \end{cases}$$

In both cases, the eigenvalues are real. On the other hand, if the argument of the square root in (3.4) is negative, then the eigenvalues form a complex conjugate pair. This is the case if

$$-\frac{-1 - \sqrt{(\tau^2 - 1)(\tau'^2 - 1)}}{\tau\tau'} < \cos \vartheta < \frac{-1 + \sqrt{(\tau^2 - 1)(\tau'^2 - 1)}}{\tau\tau'}.$$

Hence $\mathcal{L}(F_\tau(\vec{x}), F_{\tau'}(\vec{x}')) > 0$ only if the angle ϑ lies outside this interval. In this case, the relation

$$\lambda_1 \lambda_2 = \frac{1}{16} (\tau^2 - 1)(\tau'^2 - 1) > 0 \quad (3.8)$$

shows that the eigenvalues have the same sign. Therefore,

$$\mathcal{L}((\tau, \vec{x}), (\tau', \vec{x}')) = \frac{1}{2} (|\lambda_1| - |\lambda_2|)^2 = \frac{1}{2} (\lambda_1 - \lambda_2)^2. \quad (3.9)$$

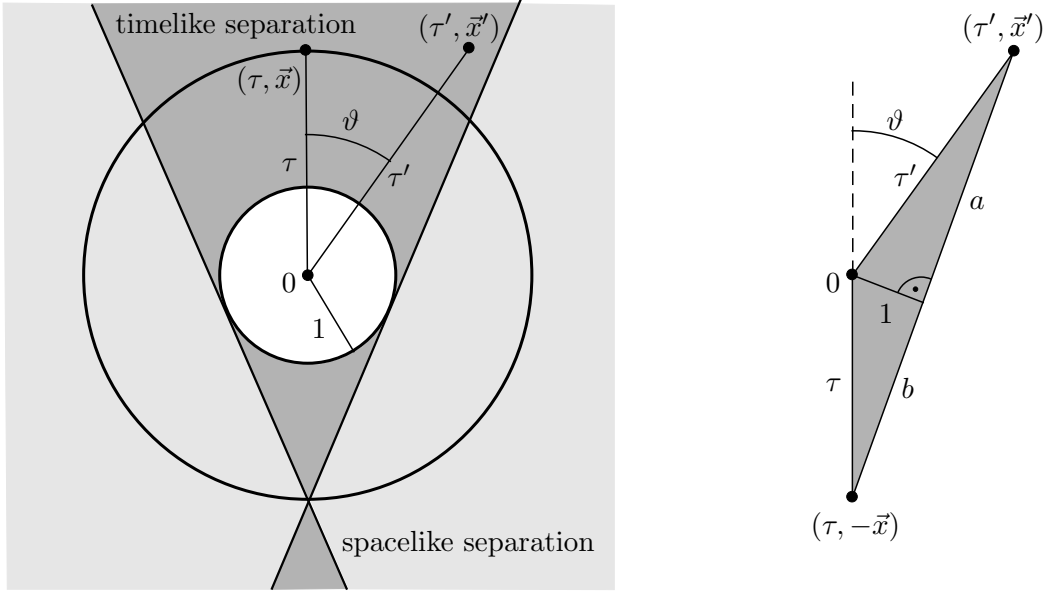
Substituting the formula for the eigenvalues (3.4) gives (3.5). \square

We next analyze the *causal relations* as introduced abstractly before (2.7). According to the explicit formula (3.4), the eigenvalues are either both real and have the same sign (see (3.8)), or else they form a complex conjugate pair. These two cases correspond precisely to *timelike* and *spacelike* separation, whereas *lightlike* separation is the boundary case of a single degenerate eigenvalue. Lightlike separation occurs when the discriminant in (3.4) vanishes, i.e. if

$$(1 + \tau\tau' \cos \vartheta)^2 = (\tau^2 - 1)(\tau'^2 - 1). \quad (3.10)$$

This equation has a simple geometric interpretation shown in Figure 1. In this figure, the points parametrized by (τ, \vec{x}) and (τ', \vec{x}') are shown, and ϑ is again the angle between \vec{x} and \vec{x}' . Given (τ, \vec{x}) , all the points (τ', \vec{x}') with timelike separation form a region of the form of a three-dimensional double cone, with the ball of radius one removed. The antipodal point $(\tau, -\vec{x})$ is the apex of this cone, and its boundary is tangential to the sphere of radius one. This causal structure can be derived using elementary trigonometry. We here explain the main step, which consists in verifying that the points with lightlike separation (3.10) form the boundary of the cone. To this end, we consider the triangle formed of the origin, the point (τ', \vec{x}') and the antipodal point of (τ, \vec{x}) (see the right of Figure 1). We only consider the case $\vartheta < \pi/2$, noting that the case $\vartheta > \pi/2$ is analogous. Applying the law of cosines to this triangle gives

$$(a + b)^2 = \tau^2 + \tau'^2 - 2\tau\tau' \cos(\pi - \vartheta) = \tau^2 + \tau'^2 + 2\tau\tau' \cos \vartheta. \quad (3.11)$$

FIGURE 1. Causal structure on \mathcal{F} in the case $f = 2$.

On the other hand, the Pythagorean theorem yields $a = \sqrt{\tau'^2 - 1}$ and $b = \sqrt{\tau^2 - 1}$, and thus

$$(a + b)^2 = \tau^2 + \tau'^2 - 2 + 2\sqrt{(\tau^2 - 1)(\tau'^2 - 1)}. \quad (3.12)$$

Combining (3.11) and (3.12) gives (3.10).

3.2. Qualitative Description of Underlying Mechanisms. The causal structure shown in Figure 1 also gives a good intuitive understanding of the causal action principle, as we now explain. The Lagrangian in the causal action (2.6) can be regarded as a *non-local potential* describing a “pair interaction” of the points $x, y \in M$ (with M according to (2.7)). Since the Lagrangian is non-negative, this non-local potential is *repulsive*. Moreover, this non-local potential vanishes unless the points are timelike separated. Therefore, in simple terms, the causal action principle aims for reaching a configuration where as many pairs of points as possible are spacelike separated. Since the opening angle of the light cone becomes smaller when τ is increased (as one sees in Figure 1 if the outer circle is made large), aiming for spacelike separation also leads to the tendency to increase τ and τ' . However, there is another competing effect: Every point $x \in M$ also contributes to the causal action via the pair interaction with itself. This *self-contribution* can be computed by evaluating (3.5) in the case $\tau' = \tau$ and $\vec{x}' = \vec{x}$,

$$\mathcal{L}((\tau, \vec{x}), (\tau, \vec{x})) = \frac{1}{8} \left((1 + \tau^2)^2 - (\tau^2 - 1)^2 \right) = \frac{\tau^2}{2}. \quad (3.13)$$

The resulting contribution to the causal action gets larger if τ is increased. As a consequence of these competing effects, the parameter τ should get large, but not too large.

This qualitative consideration conveys the correct intuition, but it does not explain how minimizers should look like. To this end, we need finer and more quantitative arguments as given in the next sections.

3.3. Minimizing in the Class of Isotropic Measures. As a first step towards the quantitative analysis, we want to shed light on the angular distribution of the points x_i for minimizing configurations. Since the variational principle is spherically symmetric, it is natural to expect that, in the limit $m \rightarrow \infty$, minimizing measures should also have this property. We refer to measures with spherical symmetry as *isotropic measures*. They can be written as

$$d\rho = \frac{1}{4\pi} d\mu(\tau) d\cos\vartheta d\varphi, \quad (3.14)$$

where μ is a normalized measure on $[1, \infty)$,

$$\int_1^\infty d\mu = 1$$

(more precisely, μ should be a regular Borel measure; for technical simplicity, the reader may restrict attention to the case $d\mu = h(\tau) d\tau$ with h a non-negative continuous function). Clearly, such a measure is *not* a weighted counting measure (see (2.3)), but it can be approximated by such measures in the weak sense.

Proposition 3.2. *For an isotropic measure (3.14), the causal action can be written as*

$$\mathcal{S}(\rho) = \int_1^\infty d\mu(\tau) \int_1^\infty d\mu(\tau') \mathcal{L}_{\text{iso}}(\tau, \tau') \quad \text{with} \quad (3.15)$$

$$\mathcal{L}_{\text{iso}}(\tau, \tau') = \frac{(\tau^2 - 1)^{\frac{3}{2}} (\tau'^2 - 1)^{\frac{3}{2}}}{12 \tau \tau'} - \frac{\tau^2 \tau'^2}{12} + \frac{\tau^2 + \tau'^2}{8}. \quad (3.16)$$

Moreover, the isotropic Lagrangian \mathcal{L}_{iso} is bounded from below by

$$\mathcal{L}_{\text{iso}}(\tau, \tau') > \mathcal{L}_{\text{iso}}(1, 1) = \frac{1}{6} \quad \text{for all } \tau, \tau' \in [1, \infty) \text{ with } (\tau, \tau') \neq (1, 1). \quad (3.17)$$

Proof. The Lagrangian \mathcal{L}_{iso} is obtained from (3.5) by integrating over ϑ . More precisely,

$$\mathcal{L}_{\text{iso}}(\tau, \tau') = \frac{1}{16} \left(\int_{-1}^{\cos\vartheta_-} + \int_{\cos\vartheta_+}^1 \right) \left((1 + \tau\tau' \cos\vartheta)^2 - (\tau^2 - 1)(\tau'^2 - 1) \right) d\cos\vartheta,$$

and a direct computation using (3.6) yields (3.16). Evaluating this formula for the isotropic Lagrangian in the case $\tau = \tau' = 1$ gives the equality in (3.17).

It remains to prove the inequality in (3.17). A simple way to verify this inequality is to plot the isotropic Lagrangian numerically, showing that $\tau = \tau' = 1$ is indeed the unique minimum. For the rigorous derivation of this inequality, by symmetry it suffices to consider the case $\tau' \geq \tau$. In the case $\tau = \tau'$, the isotropic Lagrangian simplifies to

$$\mathcal{L}_{\text{iso}}(\tau, \tau) = \frac{1}{4} - \frac{1}{12\tau^2}, \quad (3.18)$$

which clearly satisfies (3.17). Therefore, it remains to consider the case

$$\tau' > \tau.$$

We introduce the function

$$g(\tau) := \frac{\sqrt{\tau^2 - 1}}{\tau - \frac{1}{2\tau}}.$$

This function is strictly monotone increasing on $[1, \infty)$, as one readily sees by computing its derivative and verifying that it is everywhere positive. Hence we may estimate the isotropic Lagrangian by

$$\mathcal{L}_{\text{iso}}(\tau, \tau') > \frac{(\tau^2 - 1)^{\frac{3}{2}} (\tau'^2 - 1)^{\frac{3}{2}}}{12 \tau \tau'} \frac{g(\tau)}{g(\tau')} - \frac{\tau^2 \tau'^2}{12} + \frac{\tau^2 + \tau'^2}{8}.$$

In this way, the non-integer powers disappear. Next, it is convenient to introduce the new variables

$$X := \tau^2 - \frac{1}{2} \quad \text{and} \quad Y := \tau'^2,$$

which lie in the range

$$X \geq \frac{1}{2} \quad \text{and} \quad Y \geq X + \frac{1}{2}. \quad (3.19)$$

A direct computation (which we carried out with the help of computer algebra) gives

$$\mathcal{L}_{\text{iso}}(\tau, \tau') > \frac{Y}{48 X} + \frac{3}{16} - \frac{1}{32 X} + \frac{X}{24 Y} - \frac{1}{24 Y} + \frac{1}{96 X Y}.$$

In the first summand, we use the second inequality in (3.19). We thus obtain

$$\mathcal{L}_{\text{iso}}(\tau, \tau') > g(X, Y) := \frac{5}{24} - \frac{1}{48 X} + \frac{X}{24 Y} - \frac{1}{24 Y} + \frac{1}{96 X Y}.$$

Differentiating the function g with respect to X ,

$$\frac{\partial g(X, Y)}{\partial X} = \frac{4X^2 + 2Y - 1}{96 X^2 Y} > 0,$$

one sees that g is monotone increasing in X . This gives rise to the estimate

$$\mathcal{L}_{\text{iso}}(\tau, \tau') > g\left(\frac{1}{2}, Y\right) = \frac{1}{6},$$

concluding the proof. \square

The lower bound for the Lagrangian (3.17) immediately gives a corresponding lower bound for the causal action,

$$\mathcal{S}(\rho) \geq \frac{1}{6} \quad \text{for isotropic measures (3.14)}. \quad (3.20)$$

Moreover, the estimate (3.17) shows that, varying within the class of isotropic measures, the measure supported at $\tau = 1$,

$$d\rho = \frac{1}{4\pi} \delta(\tau - 1) d\tau d\cos\vartheta d\varphi \quad (3.21)$$

is the unique minimizer. In the next section, we shall show by direct computation that non-isotropic measures give rise to causal actions which are strictly smaller than $1/6$. In other words, isotropic measures are *not* minimizing. Before entering this analysis, we mention a few previous related results. For the measure (3.21), the causal action was already computed in [11, Section 1.4]. In [19, Sections 2 and 5], a detailed analysis was given for the so-called *causal variational principle on the sphere*, where one restricts attention to measures supported on a sphere of fixed radius $\tau = \tau_0$. In particular, in [19, Section 5.2] the isotropic measure on the sphere was considered,

$$d\rho = \frac{1}{4\pi} \delta(\tau - \tau_0) d\tau d\cos\vartheta d\varphi.$$

The corresponding causal action was computed, in agreement with the formula (3.18) for the isotropic Lagrangian in the case $\tau = \tau'$ (when comparing our formulas with

those in [19], one must keep in mind that in the latter paper the normalization convention for the trace (2.2) is different by assuming that this trace equals two; as a consequence, the causal Lagrangian becomes larger by an overall factor of 16).

3.4. The Two-Dimensional Discrete Dirac Sphere. We now explain how to construct measures whose causal action is strictly smaller than the lower bound $1/6$ obtained for isotropic measures (see (3.20)). We again consider a normalized weighted counting measure (see (2.3) and (2.2)). We choose the radial coordinates of all points equal to $\tau_i = \tau$. In other words, we distribute the points on a sphere of radius τ . The resulting causal variational principle on there sphere was introduced in [11, Example 2.8] and analyzed further in [19]. This analysis revealed that, in order to make the causal action small, one should distribute the points evenly on the sphere. More precisely, we choose the so-called *Tammes distribution* where one maximizes the minimal distance ϑ_m between any pair of points,

$$\vartheta_m := \min_{i,j=1,\dots,m} \arccos(\vec{x}_i \cdot \vec{x}_j)$$

(for details on the Tammes distribution see [30] or [31] and the references therein). Moreover, one chooses τ such that the opening angle of the light cone coincides with ϑ_m . Thus, evaluating (3.6) in the case $\tau = \tau'$, we choose

$$\vartheta_m = \vartheta_- = \arccos\left(1 - \frac{2}{\tau^2}\right). \quad (3.22)$$

This choice has the effect that all distinct points are spacelike separated, implying that it suffices to consider the pair interaction of each point with itself, i.e.

$$\mathcal{S}(\rho) = \sum_{i=1}^m c_i^2 \mathcal{L}((\tau, \vec{x}_i), (\tau, \vec{x}_i)).$$

Finally, we choose all the weight factors equal to $1/m$,

$$\mathcal{S}(\rho) = \frac{1}{m^2} \sum_{i=1}^m \mathcal{L}((\tau, \vec{x}_i), (\tau, \vec{x}_i)).$$

Asymptotically for large m , the Tammes distribution goes over to the densest sphere packing in \mathbb{R}^2 with the radius of the spheres given by $\vartheta_-/2$. This makes it possible to compute the causal action asymptotically.

Proposition 3.3. (The two-dimensional discrete Dirac sphere) *Choosing the points on the sphere of radius τ according to the Tammes distribution with $\vartheta_m = \vartheta_-$, the parameter τ and the causal action have the following asymptotics for large m ,*

$$\tau = \frac{\sqrt[4]{3}}{\sqrt{2\pi}} \sqrt{m} + \mathcal{O}\left(\frac{1}{\sqrt{m}}\right) \quad (3.23)$$

$$\mathcal{S} = \frac{\sqrt{3}}{4\pi} + \mathcal{O}\left(\frac{1}{m}\right). \quad (3.24)$$

Proof. The packing density δ_2 of the densest sphere packing in \mathbb{R}^2 is given by (see [8, Section 1.5])

$$\delta_2 = \frac{\pi}{6} \sqrt{3}.$$

As a consequence, the number m of circles of radius $\vartheta_-/2$ which can be distributed on the unit sphere S^2 is given asymptotically by

$$\begin{aligned} m &= \frac{\delta_2 \mu(S^2)}{\mu(B_{\vartheta_-/2}^2)} \left(1 + \mathcal{O}(\vartheta_-)\right) = \frac{\pi}{6} \sqrt{3} \frac{4\pi}{\pi(\vartheta_-/2)^2} + \mathcal{O}\left(\frac{1}{\vartheta_-}\right) \\ &= \frac{8\pi}{\sqrt{3}} \frac{1}{\vartheta_-^2} + \mathcal{O}\left(\frac{1}{\vartheta_-}\right). \end{aligned} \quad (3.25)$$

Next, using (3.22),

$$1 - \frac{2}{\tau^2} = \cos \vartheta_- = 1 - \frac{\vartheta_-^2}{2} + \mathcal{O}(\vartheta_-^4) \quad (3.26)$$

and thus

$$\vartheta_- = \frac{2}{\tau} + \mathcal{O}\left(\frac{1}{\tau^2}\right).$$

Using this expansion in (3.25), we conclude that

$$\tau^2 = \frac{\sqrt{3}}{2\pi} m + \mathcal{O}(m^0).$$

For this configuration, we only get contributions to the causal action if $x_i = x_j$. Thus

$$\mathcal{S} = \frac{1}{m^2} \sum_{i=1}^m \mathcal{L}(F_\tau(\vec{x}_i), F_\tau(\vec{x}_i)) = \frac{1}{m} \frac{\tau^2}{8} 2 \cdot 2 = \frac{\tau^2}{2m} = \frac{\sqrt{3}}{4\pi} + \mathcal{O}\left(\frac{1}{m}\right),$$

concluding the proof. \square

Comparing the asymptotics (3.24) with the estimate (3.20) and using that

$$0.138 \approx \frac{\sqrt{3}}{4\pi} < \frac{1}{6} \approx 0.167,$$

we conclude that, for large m , the absolute minimizer of the causal action principle cannot be isotropic. This result generalizes previous finding for the variational principle on the sphere in [19]; see also the finer analytic results in [3].

Another point of interest, which will also be important in our numerical analysis, is that, according to (3.23), the parameter τ tends to infinity as $m \rightarrow \infty$. In other words, the larger we choose m , the larger the radius of the discrete Dirac sphere of minimal action gets. This finding corresponds to a *non-compactness* of the causal action principle as first observed in [11, Section 2.2], which can be stated mathematically that a minimizing sequence of the causal action may diverge in the sense that the support of the measures tends to infinity. In order to gain compactness, in [11, 12] the *boundedness constraint* (2.8) was introduced. In our setting, the necessity of the boundedness constraint corresponds to the fact that, analyzing sequences of minimizing measure $(\rho_\ell)_{\ell \in \mathbb{N}}$ asymptotically as $m \rightarrow \infty$, these sequences of measures will typically diverge, while the functional \mathcal{T} in (2.8) will tend to infinity.

With this in mind, we now compute the functional \mathcal{T} for the discrete Dirac sphere.

Proposition 3.4. *For the measure describing the two-dimensional discrete Dirac sphere in Proposition 3.3, the functional \mathcal{T} in (2.8) has the asymptotics*

$$\mathcal{T} = \frac{3}{16\pi^2} m^2 + \mathcal{O}(m).$$

Proof. Again using the bijection (3.2) in order to parametrize the points of \mathcal{F} by (τ, \vec{x}) , functional \mathcal{T} becomes

$$\mathcal{T}(\rho) = \int d\rho(\tau, \vec{x}) \int d\rho(\tau', \vec{y}) (|\lambda_1| + |\lambda_2|)^2,$$

where $\lambda_{1,2}$ are the eigenvalues of the product $F_\tau(\vec{x})F_{\tau'}(\vec{x}')$ in (3.4). If the points (τ, \vec{x}) and (τ', \vec{x}') are *spacelike* or *lightlike* separated, these eigenvalues form a complex conjugate pair (because the square root is zero or imaginary). Hence, in this case,

$$(|\lambda_1| + |\lambda_2|)^2 = 4|\lambda_1|^2 = 4\lambda_1\lambda_2 \stackrel{(3.8)}{=} \frac{1}{4}(\tau^2 - 1)(\tau'^2 - 1).$$

On the other hand, if the points are *timelike* separated, both eigenvalues are real and have the same sign. Therefore,

$$(|\lambda_1| + |\lambda_2|)^2 = (\lambda_1 + \lambda_2)^2 = \left(\text{tr} (F_\tau(\vec{x}) F_\tau(\vec{y})) \right)^2 \stackrel{(3.7)}{=} \frac{1}{4} (1 + \tau\tau' \cos \vartheta)^2.$$

As in Proposition 3.3, we now choose the weights $c_i = 1/m$, and the \vec{x}_i such that all distinct points are spacelike separated. Then every single point contributes $(1 + \tau^2)^2/4$ to the \mathcal{T} , whereas each (ordered) pair of different points contributes $(\tau^2 - 1)^2/4$. Thus

$$\mathcal{T}(\rho) = \frac{1}{m^2} \left(m \frac{(1 + \tau^2)^2}{4} + m(m-1) \frac{(\tau^2 - 1)^2}{4} \right) = \frac{(\tau^2 - 1)^2}{4} + \frac{\tau^2}{m},$$

which shows that, up to a term of order $\mathcal{O}(m^{-1})$, the boundedness constraint is determined by pairs of point with spacelike separation. Employing the asymptotics for τ in (3.23) gives the result. \square

3.5. Causally Trivial Measures as Local Minimizers. In the example of the two-dimensional discrete Dirac sphere (see Proposition 3.3), all distinct spacetime points are spacelike or lightlike separated, i.e.

$$\mathcal{L}(x_i, x_j) = 0 \quad \text{for all } i \neq j.$$

We refer to a measure ρ with this property as being *causally trivial*. We conjecture that if the dimension f of the Hilbert space is sufficiently small, then every minimizing measure should be causally trivial. If f is sufficiently large, however, the causal structure of minimizing measures should become non-trivial. As a first step towards testing this conjecture, in this section we conclude the analysis in the case $f = 2$ by explaining a mechanism which shows why causally trivial measures give rise to local minima of the causal action.

Again using the identification (3.2), we write the measure (2.4) as

$$\rho = \sum_{i=1}^m c_i \delta_{F_{\tau_i}(\vec{x}_i)}.$$

If this measure is causally trivial, in the causal action only the summands with $i = j$ contribute,

$$\mathcal{S}(\rho) = \sum_{i=1}^m c_i^2 \mathcal{L}((\tau_i, \vec{x}_i), (\tau_i, \vec{x}_i)) = \sum_{i=1}^m c_i^2 \frac{\tau_i^2}{2},$$

where in the last step we applied (3.13). The weights c_i can be determined by minimizing the causal action under variations under the constraints (2.2). Using the Lagrange multiplier method, one readily finds the optimal weights

$$c_i = \frac{1}{\tau_i^2} \left(\sum_{j=1}^m \frac{1}{\tau_j^2} \right)^{-1}. \quad (3.27)$$

As a consequence, the causal action simplifies to

$$\mathcal{S}(\rho) = \frac{1}{2} \left(\sum_{i=1}^m \frac{1}{\tau_i^2} \right)^{-1}.$$

We shall now give a sufficient condition for such measures to be local minimizers of the causal action. To this end, we introduce the following notion.

Definition 3.5. *A point (τ_i, \vec{x}_i) in spacetime $M := \text{supp } \rho$ of a causally trivial measure ρ is said to be **angular lightlike restricted** if there exists an open neighborhood $U \subset S^2$ of \vec{x}_i such that for all $\vec{y} \in U$ the point (τ_i, \vec{y}) is timelike separated from at least one point in $M \setminus \{(\tau_i, \vec{x}_i)\}$.*

Intuitively speaking, angular lightlike restriction means that the angular coordinate $\vec{x}_i \in S^2$ of a point $(\tau_i, \vec{x}_i) \in \mathcal{F}$ cannot be varied without the point entering the light cone of another spacetime point.

Proposition 3.6. *Let ρ be a causally trivial measure with optimal weights (3.27). Assume that every spacetime point (τ_i, \vec{x}_i) in $\text{supp } \rho$ is angular lightlike restricted and lightlike separated from at least $k \geq 3$ points. Moreover, assume that the radial coordinates of all points are at least*

$$\tau_i \geq \sqrt{\frac{k}{k-2}}.$$

Then ρ is a local minimizer of the causal action principle.

Proof. We need to show that the action $\mathcal{S}(\rho)$ cannot be decreased by a small change in the free parameters, namely the weights, the angular coordinates or the radial coordinates. The weights are already chosen optimally by (3.27). Moreover, since all points are angular restricted, any non-trivial variation of the angular coordinates x_i gives rise to a strictly positive first variation of $\mathcal{S}(\rho)$. Hence it remains to show that any small change of the radial coordinates τ_i increases $\mathcal{S}(\rho)$.

The contribution from a pair of points to the total action is given in (3.5). Differentiating the self-contribution in (3.13) gives

$$\partial_{\tau_i} \mathcal{L}(F_{\tau_i}(\vec{x}_i), F_{\tau_i}(\vec{x}_i)) = \tau_i.$$

Thus the self-contribution becomes smaller when the radial coordinate of a point is decreased. We next consider a pair of points (τ, \vec{x}) and (τ', \vec{x}') which are lightlike separated and such that the angle ϑ between \vec{x} and \vec{x}' is smaller than $\frac{\pi}{2}$, i.e., according to (3.6),

$$\cos \vartheta = \cos \vartheta_- = \frac{1}{\tau \tau'} \left(\sqrt{(\tau^2 - 1)(\tau'^2 - 1)} - 1 \right).$$

In this case, the contribution $\mathcal{L}(F_\tau(\vec{x}), F_{\tau'}(\vec{x}'))$ to the causal action vanishes. This term remains zero if either of the radial coordinates are *increased*. Hence the one-sided derivative, corresponding to an increase of the radial coordinate, vanishes:

$$\left. \frac{\partial}{\partial \epsilon} \right|_{\epsilon \geq 0} \mathcal{L}((\tau + \epsilon, \vec{x}), (\tau', \vec{x}')) = 0.$$

If, however, the radial coordinate of one point is *decreased*, we obtain

$$\begin{aligned} \left. \frac{\partial}{\partial \epsilon} \right|_{\epsilon \geq 0} \mathcal{L}((\tau - \epsilon, \vec{x}), (\tau', \vec{x}')) &= -\frac{1}{8} \frac{\partial}{\partial \tau} \left((1 + \tau \tau' \cos \vartheta_-)^2 - (\tau^2 - 1)(\tau'^2 - 1) \right) \\ &= \frac{\sqrt{\tau'^2 - 1}}{4\tau} \left(\sqrt{\tau'^2 - 1} + \sqrt{\tau^2 - 1} \right). \end{aligned}$$

Now consider an arbitrary spacetime point $(\tau_i, \vec{x}_i) \in \text{supp } \rho$ and let $\{(\tau_j, \vec{x}_j) \mid j \in J\}$ be the set of points which are lightlike separated from (τ_i, \vec{x}_i) . (By assumption we have $\#J \geq k$, i.e. J contains at least k elements.) Then the one-sided derivative of the total action when decreasing the radial coordinate τ_i is given by

$$\begin{aligned} \left. \frac{\partial}{\partial \epsilon} \right|_{\epsilon \geq 0} c_i^2 \mathcal{L}((\tau_i - \epsilon, \vec{x}_i), (\tau_i - \epsilon, \vec{x}_i)) &+ 2c_i \sum_{j \in J} c_j \mathcal{L}((\tau_i - \epsilon, \vec{x}_i), (\tau_j, \vec{x}_j)) \\ &= -c_i^2 \tau_i + 2c_i \sum_{j \in J} c_j \frac{\sqrt{\tau_j^2 - 1}}{4\tau_i} \left(\sqrt{\tau_j^2 - 1} + \sqrt{\tau_i^2 - 1} \right) \\ &= \left(\sum_{k=1}^m \frac{1}{\tau_k^2} \right)^{-2} \left\{ -\frac{1}{\tau_i^3} + 2 \sum_{j \in J} \frac{1}{\tau_i^2 \tau_j^2} \frac{\sqrt{\tau_j^2 - 1}}{4\tau_i} \left(\sqrt{\tau_j^2 - 1} + \sqrt{\tau_i^2 - 1} \right) \right\} \\ &> \left(\sum_{k=1}^m \frac{1}{\tau_k^2} \right)^{-2} \frac{1}{\tau_i^3} \left\{ -1 + \sum_{j \in J} \frac{\sqrt{\tau_j^2 - 1}}{2\tau_j^2} \sqrt{\tau_j^2 - 1} \right\} \\ &= \left(\sum_{k=1}^m \frac{1}{\tau_k^2} \right)^{-2} \frac{1}{\tau_i^3} \left\{ -1 + \sum_{j \in J} \left(\frac{1}{2} - \frac{1}{2\tau_j^2} \right) \right\} \\ &\geq \left(\sum_{k=1}^m \frac{1}{\tau_k^2} \right)^{-2} \frac{1}{\tau_i^3} \left\{ -1 + k \left(\frac{1}{2} - \frac{k-2}{2k} \right) \right\} = 0. \end{aligned}$$

Hence the variation is strictly positive, concluding the proof. \square

4. THE FOUR-DIMENSIONAL DISCRETE DIRAC SPHERE

In the previous section, we considered the simplest interesting case $n = 1$ and $f = 2$. For physically interesting models one should choose the dimension f of the Hilbert space \mathcal{H} to be very large. Moreover, in order to model Dirac spinors, one should choose the spin dimension $n = 2$. The resulting higher-dimensional causal fermion systems are much more difficult to analyze, mainly because the dimension of the space \mathcal{F} of linear operators gets large (more precisely, the operators with n positive and n negative eigenvalues and prescribed trace form a manifold of dimension $4nf - 4n^2 - 1$; see [15, Theorem 3.2]). In particular, one no longer has the simple representation of

the operators in \mathcal{F} in terms of Pauli matrices (3.2). For this reason, there are hardly any analytic results, making it necessary to explore the situation numerically.

However, there are higher-dimensional analogs of the discrete Dirac spheres of Proposition 3.3. In the case $n = 2$ and $f = 4$, the resulting causal fermion systems will serve as test cases for the numerics. We conjecture that, asymptotically for large m , minimizers of the causal action principle should be close to these discrete Dirac spheres. Compared to the two-dimensional case, there is the additional feature that the causal action tends to zero if $m \rightarrow \infty$ (see Proposition 4.2). The resulting sequence of measures again diverges, in agreement with our discussion of the boundedness constraint at the end of Section 3.4. The new feature is that there are divergent minimizing sequences whose causal action tends to zero.

We now introduce the four-dimensional discrete Dirac sphere in detail, based on a related continuous system introduced in [11, Example 2.9] (the so-called three-dimensional Dirac sphere). Let $\mathcal{H} = \mathbb{C}^4$. We introduce five 4×4 -matrices acting on \mathcal{H} by

$$\gamma^\alpha = \begin{pmatrix} \sigma^\alpha & 0 \\ 0 & -\sigma^\alpha \end{pmatrix}, \quad \alpha = 1, 2, 3, \quad \gamma^4 = \begin{pmatrix} 0 & i \mathbf{1} \\ -i \mathbf{1} & 0 \end{pmatrix} \quad \text{and} \quad \gamma^5 = \begin{pmatrix} 0 & \mathbf{1} \\ \mathbf{1} & 0 \end{pmatrix}$$

(where the σ^α are again the Pauli matrices (3.1)). Given a parameter $\tau > 1$, we consider the following mapping from the sphere $S^4 \subset \mathbb{R}^5$ to the linear operators on \mathcal{H} ,

$$F : S^4 \rightarrow L(\mathcal{H}), \quad F(x) = \frac{1}{4} \left(\sum_{i=1}^5 \tau x^i \gamma^i + \mathbf{1} \right).$$

Choosing m points $x_1, \dots, x_m \in S^4$ on the sphere, we again introduce ρ as the normalized weighted counting measure (2.3).

Let us verify that the matrix $F(x)$ lies in \mathcal{F} : First, this matrix is obviously symmetric and has trace one. In order to compute its eigenvalues, it is most convenient to make use of the fact that the matrices γ^j are the Dirac matrices of Euclidean \mathbb{R}^5 , satisfying the anti-commutation relations

$$\{\gamma^i, \gamma^j\} = 2\delta^{ij} \mathbf{1} \quad (i, j = 1, \dots, 4).$$

As a consequence,

$$\begin{aligned} 4F(x) - \mathbf{1} &= \sum_{i=1}^5 \tau x^i \gamma^i \\ (4F(x) - \mathbf{1})^2 &= \sum_{i,j=1}^5 \tau^2 x^i x^j \gamma^i \gamma^j = \frac{\tau^2}{2} \sum_{i,j=1}^5 x^i x^j \{\gamma^i, \gamma^j\} \\ &= \frac{\tau^2}{2} \sum_{i,j=1}^5 x^i x^j 2\delta_{ij} \mathbf{1} = \tau^2 \mathbf{1}. \end{aligned}$$

Hence the matrix $F(x)$ satisfies the polynomial equation

$$(4F(x) - \mathbf{1})^2 = \tau^2 \mathbf{1}.$$

We conclude that $F(x)$ has the eigenvalues

$$\nu_{\pm} = \frac{1}{4} (1 \pm \tau).$$

Moreover, since the matrix $4F(x) - \mathbf{1}$ is trace-free, each eigenvalue must appear with multiplicity two. We conclude that $F(x) \in \mathcal{F}$ if we choose the spin dimension $n = 2$.

We next compute the Lagrangian.

Lemma 4.1. *Denoting the angle between the vectors $x, y \in \mathbb{R}^5$ by ϑ ,*

$$\mathcal{L}(F(x), F(y)) = \frac{\tau^2}{64} (1 + \cos \vartheta) (2 - \tau^2 (1 - \cos \vartheta)) \Theta(\vartheta_{\max} - \vartheta),$$

where

$$\vartheta_{\max} := \arccos\left(1 - \frac{2}{\tau^2}\right). \quad (4.1)$$

Proof. Let us compute the eigenvalues of the operator product $F(x)F(y)$. Again, it is most convenient to make use of the Clifford relations. First,

$$\begin{aligned} 16 F(x) F(y) &= \left(\sum_{i=1}^5 \tau x^i \gamma^i + \mathbf{1} \right) \left(\sum_{j=1}^5 \tau y^j \gamma^j + \mathbf{1} \right) \\ &= (1 + \tau^2 \langle x, y \rangle) \mathbf{1} + \tau \sum_{k=1}^5 (x^k + y^k) \gamma^k + \frac{\tau^2}{2} \sum_{i,j=1}^5 x^i y^j [\gamma^i, \gamma^j]. \end{aligned} \quad (4.2)$$

Using that

$$\gamma^i [\gamma^i, \gamma^j] = -[\gamma^i, \gamma^j] \gamma^i,$$

we conclude that

$$\left(16 F(x) F(y) - (1 + \tau^2 \langle x, y \rangle) \mathbf{1} \right)^2 = \tau^2 \sum_{k=1}^5 (x^k + y^k)^2 \mathbf{1} + \left(\frac{\tau^2}{2} \sum_{i,j=1}^5 x^i y^j [\gamma^i, \gamma^j] \right)^2.$$

This can be simplified with the help of the relations

$$\sum_{i=1}^5 (x^i + y^i)^2 = 2 + 2 \langle x, y \rangle \quad (4.3)$$

$$\left(\sum_{i,j=1}^5 x^i y^j [\gamma^i, \gamma^j] \right)^2 = -4 \sin^2 \vartheta \mathbf{1} = -4 (1 - \langle x, y \rangle^2) \mathbf{1}, \quad (4.4)$$

where ϑ is the angle between the vectors $x, y \in \mathbb{R}^5$. The relation (4.4) can be verified in detail as follows. The rotational symmetry of the Euclidean Dirac operator on \mathbb{R}^5 means that for every rotation $O \in \text{SO}(5)$ there is a unitary operator $U \in \text{SU}(4)$ such that

$$O_j^i \gamma^j = U \gamma^i U^{-1}$$

(more details can be found in the three-dimensional case in [32, Section 1] and in four dimensions in [32, Section 2.1], [6, Section 2.2] or [27, eq. (3.29)]; the five-dimensional case considered here is similar). Making use of this rotational symmetry, we can arrange that the vector x is the basis vector e_1 and that $y = \cos \vartheta e_1 + \sin \vartheta e_2$. As a

consequence,

$$\begin{aligned} \sum_{i,j=1}^5 x^i y^j [\gamma^i, \gamma^j] &= \sin \vartheta [\gamma^1, \gamma^2] = 2 \sin \vartheta \gamma^1 \gamma^2 \\ \left(\sum_{i,j=1}^5 x^i y^j [\gamma^i, \gamma^j] \right)^2 &= 4 \sin^2 \vartheta \gamma^1 \gamma^2 \gamma^1 \gamma^2, \end{aligned}$$

and applying the anti-commutation relations gives (4.4).

Combining the above equations, we conclude that the product $F(x) F(y)$ satisfies the polynomial equation

$$\begin{aligned} \left(16 F(x) F(y) - (1 + \tau^2 \langle x, y \rangle) \mathbf{1} \right)^2 &= 2 \tau^2 (1 + \langle x, y \rangle) \mathbf{1} - \tau^4 (1 - \langle x, y \rangle)^2 \mathbf{1} \\ &= \tau^2 \left(1 + \langle x, y \rangle \right) \left(2 - \tau^2 (1 - \langle x, y \rangle) \right) \mathbf{1}. \end{aligned}$$

Taking the square root, the zeros of this polynomial are computed by

$$\lambda_{1/2} = \frac{1}{16} \left(1 + \tau^2 \langle x, y \rangle \pm \tau \sqrt{1 + \langle x, y \rangle} \sqrt{2 - \tau^2 (1 - \langle x, y \rangle)} \right). \quad (4.5)$$

Moreover, taking the trace of (4.2), one finds

$$\text{tr} (16 F(x) F(y)) = 4 (1 + \tau^2 \langle x, y \rangle).$$

This implies that each eigenvalue in (4.5) has algebraic multiplicity two.

After these preparations, we can compute the Lagrangian. If ϑ is sufficiently small, then the term $(1 - \langle x, y \rangle)$ in (4.5) is close to zero, and thus the arguments of the square roots are all positive. However, if ϑ becomes so large that $\vartheta \geq \vartheta_{\max}$, then the argument of the last square root in (4.5) becomes negative, so that the eigenvalues $\lambda_{1/2}$ form a complex conjugate pair. Moreover, a short calculation shows that

$$\lambda_1 \lambda_2 = \frac{1}{256} (1 + \tau)^2 (1 - \tau)^2 > 0, \quad (4.6)$$

implying that if the $\lambda_{1/2}$ are both real, then they have the same sign. Using this information in (2.5), the Lagrangian simplifies to

$$\begin{aligned} \mathcal{L}(F(x), F(y)) &= \frac{1}{8} \sum_{i,j=1}^4 \left(|\lambda_i^{xy}| - |\lambda_j^{xy}| \right)^2 = \frac{1}{2} \sum_{i,j=1}^2 \left(|\lambda_i| - |\lambda_j| \right)^2 \\ &= \frac{1}{2} \Theta(\vartheta_{\max} - \vartheta) \sum_{i,j=1}^2 \left(\lambda_i - \lambda_j \right)^2 = \Theta(\vartheta_{\max} - \vartheta) (\lambda_1 - \lambda_2)^2 \\ &= \frac{4 \tau^2}{256} (1 + \cos \vartheta) (2 - \tau^2 (1 - \cos \vartheta)) \Theta(\vartheta_{\max} - \vartheta). \end{aligned}$$

This concludes the proof. \square

Proposition 4.2. *Choosing the points on S^4 according to the Tamme distribution on the four-sphere with $\vartheta_m = \vartheta_{\max}$ and*

$$\tau = \frac{3^{\frac{1}{4}}}{\sqrt{\pi}} \sqrt[4]{m} + \mathcal{O}(m^{-\frac{3}{4}}), \quad (4.7)$$

the causal action has the asymptotics

$$\mathcal{S} = \frac{\sqrt{3}}{16\pi} \frac{1}{\sqrt{m}} + \mathcal{O}(m^{-\frac{3}{2}}).$$

Proof. The packing density δ_4 of the densest sphere packing in \mathbb{R}^4 is given by (see [8, Section 1.5])

$$\delta_4 = \frac{\pi^2}{16}.$$

Moreover, the volume $\mu(S^4)$ of the unit 4-sphere and the volume $\mu(B_r^4)$ of a 4-ball are

$$\mu(S^4) = \frac{8}{3} \pi^2 \quad \text{and} \quad \mu(B_r^4) = \frac{\pi^2}{2} r^4.$$

As a consequence, the number m of 4-balls of radius $\vartheta_{\max}/2$ which can be distributed on the unit sphere S^4 is given asymptotically by

$$\begin{aligned} m &= \frac{\delta_4 \mu(S^4)}{\mu(B_{\vartheta_{\max}/2}^4)} \left(1 + \mathcal{O}(\vartheta_{\max})\right) = \frac{\pi^2}{16} \frac{8}{3} \frac{\pi^2}{\pi^2} \frac{2}{(\vartheta_{\max}/2)^4} + \mathcal{O}\left(\frac{1}{\vartheta_{\max}^3}\right) \\ &= \frac{16\pi^2}{3} \frac{1}{\vartheta_{\max}^4} + \mathcal{O}\left(\frac{1}{\vartheta_{\max}^3}\right). \end{aligned} \quad (4.8)$$

Next, using (4.1), exactly as in (3.26) we obtain

$$\vartheta_{\max} = \frac{2}{\tau} + \mathcal{O}\left(\frac{1}{\tau^2}\right).$$

Using this expansion in (4.8), we conclude that

$$\tau^4 = \frac{3}{\pi^2} m + \mathcal{O}(m^0).$$

For this configuration, we only get contributions to the causal action if $x = y$. Thus

$$\mathcal{S} = \frac{1}{m^2} \sum_{i=1}^m \mathcal{L}(F(x_i), F(x_i)) = \frac{1}{m} \frac{\tau^2}{64} 22 = \frac{1}{16} \frac{\sqrt{3}}{\pi} \frac{1}{\sqrt{m}} + \mathcal{O}(m^{-\frac{3}{2}}).$$

This gives the result. \square

Similar as in Proposition 3.4, we finally compute the functional \mathcal{T} .

Proposition 4.3. *Choosing the points on S^4 according to the Tammes distribution on the four-sphere with $\vartheta_m = \vartheta_{\max}$ and τ according to (4.7), the functional \mathcal{T} in (2.8) has the asymptotics*

$$\mathcal{T} = \frac{1}{16} (1 + \tau)^2 (1 - \tau)^2 + \mathcal{O}\left(\frac{1}{m}\right).$$

Proof. Exactly as in the proof of Proposition 3.4, the leading contribution to \mathcal{T} comes from pairs of points with spacelike separation. In this case, the eigenvalues of the operator product $F(x)F(y)$ form a complex conjugate pair and are both two-fold degenerate. Moreover, using (4.5) and (4.6), we obtain

$$|\lambda_1|^2 = |\lambda_2|^2 = \lambda_1 \lambda_2 = \frac{1}{256} (1 + \tau)^2 (1 - \tau)^2.$$

and thus

$$\left(\sum_{i=1}^{2n} |\lambda_i^{xy}| \right)^2 = \frac{1}{16} (1 + \tau)^2 (1 - \tau)^2.$$

We now integrate over x and y and use that the pairs with timelike separation give a contribution of the order $1/m$. \square

5. CAUSAL CONES IN SPIN DIMENSION ONE

In Section 3.1 we showed that in the case $n = 1$ and $f = 2$, the causal relations give rise to cones (see Figure 1). This geometric picture extends to a general dimension f of the Hilbert space, as we now explain. While it is not possible to represent the causal relations between all points in \mathcal{F} simultaneously, the relation between one fixed point and all other points can be represented geometrically again with a double cone (see Figure 2 below). We again choose the spin dimension $n = 1$, but now with arbitrary $f \geq 2$. We denote the fixed reference point by $x \in \mathcal{F}$, and its non-trivial eigenvalues by $\nu_{\pm} = \frac{1}{2}(1 \pm \tau)$ with $\tau \geq 1$, as above. Furthermore, we denote the orthogonal projection to the two-dimensional image of x by

$$\pi_x : \mathcal{H} \rightarrow x(\mathcal{H}) \subset \mathcal{H}.$$

Let $y \in \mathcal{F}$ be arbitrary. The causal relations between x and y are determined by the eigenvalues of the product xy . These eigenvalues are equal to the eigenvalues of the operator product $x(\pi_x y \pi_x)$. Hence, in order to analyze the causal relation between x and y it suffices to investigate the projected operator $\pi_x y \pi_x$. We first derive inequalities for its eigenvalues.

Proposition 5.1. *Let $\nu'_+ > 0$ and $\nu'_- = (1 - \nu'_+) \leq 0$ denote the non-trivial eigenvalues of y . Then the eigenvalues ν'_1, ν'_2 of the operator $\pi_x y \pi_x$, ordered by size $\nu'_1 \leq \nu'_2$, satisfy the inequalities*

$$\nu'_- \leq \nu'_1 \leq 0 \leq \nu'_2 \leq \nu'_+. \quad (5.1)$$

Furthermore, the trace of the projected operator is bounded by

$$\nu'_- \leq \text{tr}(\pi_x y \pi_x) \leq \nu'_+.$$

Proof. The lemma follows readily from the min-max principle (see for example [29, Section XIII.1]). Indeed, the inequality $\nu'_2 \leq \nu'_+$ follows from the estimate

$$\nu'_+ = \sup_{0 \neq u \in \mathcal{H}} \frac{\langle u | y u \rangle_{\mathcal{H}}}{\langle u | u \rangle_{\mathcal{H}}} \geq \sup_{0 \neq u \in x(\mathcal{H})} \frac{\langle u | y u \rangle_{\mathcal{H}}}{\langle u | u \rangle_{\mathcal{H}}} = \sup_{0 \neq u \in \mathcal{H}} \frac{\langle u | \pi_x y \pi_x u \rangle_{\mathcal{H}}}{\langle u | u \rangle_{\mathcal{H}}} = \nu'_2.$$

The proof of the inequality $\nu'_- \leq \nu'_2$ is analogous.

In order to show that one eigenvalue is non-negative and the other is non-positive, we proceed indirectly. Assume conversely that both eigenvalues are for example strictly positive,

$$\nu'_1, \nu'_2 > 0.$$

Then the min-max principle implies that the operator y has at least two strictly positive eigenvalues, which is a contradiction to $y \in \mathcal{F}$.

Finally, the estimate of the trace follows immediately from the identity $\text{tr} \pi_x y \pi_x = \nu'_1 + \nu'_2$ by applying (5.1). \square

We choose an orthonormal eigenvector basis of x of the subspace $x(\mathcal{H})$. In this basis,

$$x|_{x(\mathcal{H})} = \frac{1}{2} (\mathbf{1} + \tau \sigma^3). \quad (5.2)$$

Similarly to (3.2), the operator $\pi_x y \pi_x$ can be represented in this basis in terms of four real coordinates (y_0, y_1, y_2, y_3) by the matrix

$$\pi_x y \pi_x|_{x(\mathcal{H})} = \frac{1}{2} \left(y_0 \mathbb{1} + \sum_{i=1}^3 y_i \sigma_i \right) = \frac{1}{2} \begin{pmatrix} y_0 + y_3 & y_1 - iy_2 \\ y_1 + iy_2 & y_0 - y_3 \end{pmatrix}. \quad (5.3)$$

This matrix also corresponds to the first diagonal 2×2 -block of the $f \times f$ -dimensional matrix representation of y on \mathcal{H} with respect to the eigenvector basis of x (in which the two non-trivial eigenvectors appear first). The eigenvalues of this matrix are computed by

$$\nu'_{1/2} = \frac{1}{2} (y_0 \pm |\vec{y}|)$$

(with $|\vec{y}|^2 = y_1^2 + y_2^2 + y_3^2$). In order to get agreement with the formula (3.3) in Section 3.1, we denote the eigenvalues of y by

$$\nu'_{\pm} = \frac{1}{2} (1 \pm \tau').$$

Then the inequalities (5.1) imply the side conditions

$$0 \leq y_0 + |\vec{y}| \leq 1 + \tau' \quad \text{and} \quad 1 - \tau' \leq y_0 - |\vec{y}| \leq 0. \quad (5.4)$$

on the coordinates (y_0, y_1, y_2, y_3) . This means that the allowed values of the coordinates (y_0, \vec{y}) representing the operator $\pi_x y \pi_x$, for any $y \in \mathcal{F}$ are restricted to lie inside the shaded region shown on the right of Figure 2. In particular, the allowed region lies outside the double cone defined by $|\vec{y}| \geq |y_0|$. In the following, we will see that this cone generalizes the unit circle around the origin in Figure 1, which corresponds to the hyperplane $y_0 = 1$.

The point x can be represented on $x(\mathcal{H})$ again through (3.2) by $F_{\tau}(\vec{x})$. Using this representation, the eigenvalues of the matrix $x \pi_x y \pi_x$ are computed by

$$\lambda_{1,2} = \frac{1}{4} \left(y_0 + y_3 \tau \pm \sqrt{(y_1^2 + y_2^2)(1 - \tau^2) + (y_3 + y_0 \tau)^2} \right). \quad (5.5)$$

It follows that the point y is spacelike separated from x if and only if

$$(\tau^2 - 1)(y_1^2 + y_2^2) > (y_3 + y_0 \tau)^2. \quad (5.6)$$

In every hyperplane of constant y_0 , this equation defines a double cone with apex at the point $(y_0, y_1 = y_2 = 0, y_3 = -y_0 \tau)$ and opening angle 2θ determined by the equation $\sin \theta = 1/\tau$. This means geometrically that the cone is tangent to the sphere of radius $|y_0|$ around the origin. The resulting cone in the hyperplane of constant y_0 is depicted on the left of Figure 2.

We finally remark that, using the formula for the eigenvalues (5.5), the causal Lagrangian (2.5) can be written as

$$\mathcal{L}(x, y) = \max(0, \mathcal{D}(x, y)), \quad (5.7)$$

where the function $\mathcal{D}(x, y)$ is given in analogy to (3.9) by

$$\mathcal{D}(x, y) = \frac{1}{2} (\lambda_1 - \lambda_2)^2 = \text{tr}((xy)^2) - \frac{1}{2} \text{tr}(xy)^2. \quad (5.8)$$

This form of the Lagrangian is particularly efficient for numerical calculations.

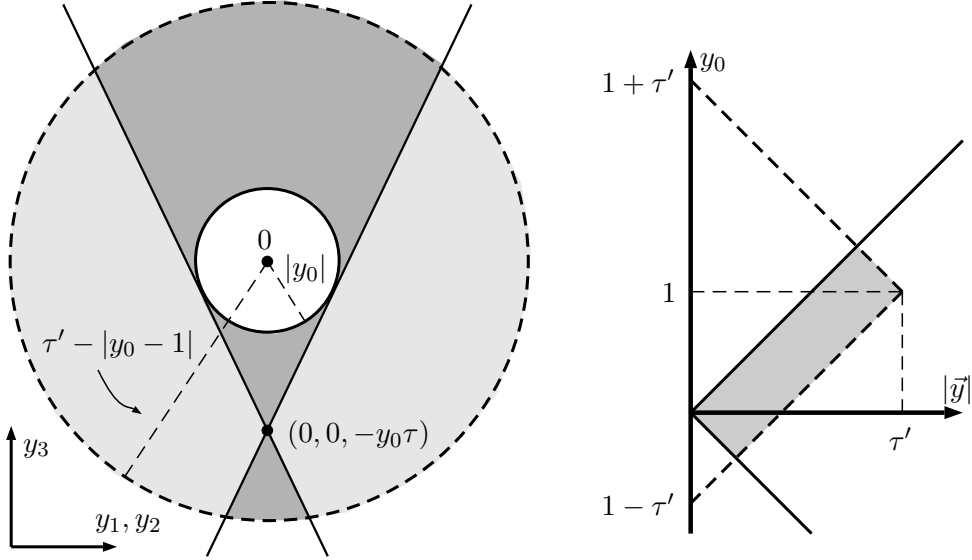


FIGURE 2. Causal cones in spin dimension one. On the right, conditions (5.4) on the coordinates (y_0, y_1, y_2, y_3) representing $\pi_x y \pi_x$ are visualized. On the left, for fixed value of y_0 the causal cone in the (y_1, y_2, y_3) -hyperplane is shown, using rotational symmetry around the y_3 -axis.

6. NUMERICAL ANALYSIS

6.1. Overview and Optimization Choices. In this section we present the numerical optimization scheme. First, we revisit the causal action principle (see (2.6)) for the weighted counting measure (2.3). We seek to solve the optimization problem

$$\begin{aligned} \text{minimize } \mathcal{S}(c_1, \dots, c_m, x_1, \dots, x_m) &= \sum_{i,j=1}^m c_i c_j \mathcal{L}(x_i, x_j) & (6.1) \\ \text{subject to } c_i &\geq 0 \text{ for all } i \in \{1, \dots, m\}, \\ \sum_{i=1}^m c_i &= 1, \\ x_i &\in \mathcal{F} \text{ for all } i \in \{1, \dots, m\}, \end{aligned}$$

where $x_i \in \mathcal{F} \subset \mathbb{C}^{f \times f}$ implies that the x_i are symmetric ($x_i^* = x_i$), have unit trace ($\text{tr } x_i = 1$), and at most n positive and at most n negative eigenvalues. Also accounting for the unit-trace requirement we have $\dim_{\mathbb{R}}(\mathcal{F}) = 4nf - 4n^2 - 1$ [15] and thus the parameter space of the optimization problem consists of

$$D' := m \cdot \dim_{\mathbb{R}}(\mathcal{F}) + m - 1 = m(4fn - 4n^2) - 1$$

real parameters.

In choosing a suitable numerical optimization scheme, we first note that the objective $\mathcal{S}(c_1, \dots, c_m, x_1, \dots, x_m)$ is non-convex and not differentiable in the x_i . However, the causal action is continuous in c_i as well as the entries of x_i with only finitely many points at which it is not differentiable. Therefore, we can in principle obtain gradients of the causal action almost everywhere.

Even though local optimization techniques are not guaranteed to converge to a global optimum for this non-convex problem, we prefer them over global schemes due to their computational efficiency in high dimensions. Specifically, since the number of optimization parameters grows linearly with m and f and we are interested in the asymptotics when m or f become large, global optimization techniques would quickly become computationally infeasible. Almost everywhere differentiability of the objective allows us to leverage gradient-information in the optimization. Recent advances in computational frameworks for gradient-based local optimization such as JAX [7] that were mostly developed for machine learning allow for efficient *automatic differentiation*, which we will describe only briefly in the following.

It would be cumbersome to compute the gradient of the objective in (6.1) analytically. However, once it is implemented numerically within a framework that allows for *differentiable programming*, the framework traces all computations performed on the input parameters and builds a computation graph of atomic operations that keeps track of how the input parameters were computationally combined to yield the scalar output \mathcal{S} . Atomic operations include arithmetic operations such as addition, subtraction, multiplication, division or powers, as well as elementary functions such as log, exp, sin, cos, ... for which derivatives are known and also implemented within the framework. If only atomic operations occur in the function implementation, the chain rule can be exploited in an automated iterative fashion (with varying degrees of optimizations) to efficiently compute the gradient of the function at any given input (see, e.g., [4] for more details). Building on these atomic building blocks, modern libraries can automatically generate gradients even for complex operations such as iterative procedures for eigenvalue computations or matrix factorization routines. Moreover, they increasingly perform low-level just-in-time compilation with various hardware-specific optimizations to speed up these gradient computations not only for specific central processing unit (CPU) architectures, but also hardware accelerators such as graphics processing units (GPU) or tensor cores [7].

With gradient information about \mathcal{S} readily available via automatic differentiation, we can directly use established optimizers such as BFGS or limited memory BFGS (L-BFGS) [26]. It has been empirically known and convincingly argued that quasi-Newton methods, in particular BFGS, often converge to local minima for non-smooth, non-convex objective functions [24, 25]. Only recently the seminal proof by Powell of the global convergence of BFGS on smooth convex functions (under mild conditions) [28] has been extended to certain non-smooth functions [20]. Given the dimensionality of our optimization problem and the structure of the objective, we choose the well-tested BFGS quasi-Newton method for optimization. The general wisdom has become that L-BFGS, a limited memory version of BFGS, is similarly reliable and greatly accelerates BFGS by maintaining a more memory-efficient representation of the approximated inverse Hessian at each optimization step. However, the current understanding is that L-BFGS may fail more regularly on non-smooth problems [2]. In our empirical evaluation, we combine L-BFGS for the first steps to quickly approach a local minimum and then switch to BFGS.

BFGS only applies to unconstrained optimization problems. While there is a variant of L-BFGS that can handle box constraints, no existing schemes can directly deal with our unit-sum constraint on c or the requirement that all x_i lie in \mathcal{F} . Therefore, we now describe how we implement the causal action numerically step by step as a function of unconstrained optimization parameters. By construction of this procedure

all constraints are satisfied automatically, reducing the degrees of freedom from a larger number of unconstrained optimization parameters back to D' .

6.2. Parametrization of the Optimization Problem. In the implementation, we optimize over the following *unconstrained* parameters

$$\tilde{c} \in \mathbb{R}^m, \mu^+ \in \mathbb{R}^{m \times n}, \mu^- \in \mathbb{R}^{m \times n}, B^1 \in \mathbb{C}^{m \times 2n \times 2n}, B^2 \in \mathbb{C}^{m \times 2n \times (f-2n)},$$

where we assume that $\Gamma_i := \sum_{l=1}^n (e^{\mu_{i,l}^+} - e^{\mu_{i,l}^-}) \geq 0$ for each $i \in \{1, \dots, m\}$ (otherwise we flip the respective superscripts \pm). With these $D = m(4fn + 2n + 1) > D'$ (for $n, f, m > 0$) free real parameters we are over-parametrizing the optimization problem in (6.1). The additional degrees of freedom will be removed in the construction of the causal action from these parameters. In the following, all assignments and conditions for optimization parameters with subscript i hold for all $i \in \{1, \dots, m\}$. Here and in what follows, the index i always refers to the numbering of the points of the weighted counting measure. In order to ensure $c_i \geq 0$ and $\sum_{i=1}^m c_i = 1$, we compute the actual weights as

$$c_i := \frac{e^{\tilde{c}_i}}{\sum_{i=1}^m e^{\tilde{c}_i}},$$

thereby eliminating one degree of freedom. Next, we compute the at most n positive and at most n negative eigenvalues of the operators x_i from the optimization parameters by

$$\nu_{i,j}^\pm := \pm \frac{e^{\mu_{i,j}^\pm}}{\Gamma_i} \quad \text{for all } i \in \{1, \dots, m\}, j \in \{1, \dots, n\}.$$

This eliminates m degrees of freedom. Finally, we construct the Hermitian matrices x_i via uniform transformations

$$x_i := U_i \text{diag}(\nu_i^+, \nu_i^-, \underbrace{0, \dots, 0}_{f-2n \text{ times}}) U_i^*,$$

where the unitary matrices U_i are in turn defined via $U_i := \exp(-i H_i)$ for Hermitian matrices

$$H_i := \begin{pmatrix} H_i^1 & B_i^2 \\ (B_i^2)^* & 0 \end{pmatrix}, \quad \text{where} \quad H_i^1 := (B_i^1 + (B_i^1)^*) \odot \begin{pmatrix} 0 & & 1 \\ & \ddots & \\ 1 & & 0 \end{pmatrix}.$$

Here, \odot denotes element-wise multiplication, i.e., H_i^1 is simply the matrix $B_i^1 + (B_i^1)^*$ with all diagonal entries set to zero (these diagonal entries describe irrelevant phase transformations and are therefore disregarded). Due to this construction, only $2n(2n-1)/2$ entries of B_i^1 remain as actual (complex) degrees of freedom, eliminating a total of $2n(2n+1)$ real degrees of freedom. Note that by construction, $x_i \in \mathcal{F}$ as the way we chose ν_i^\pm guarantees that $\text{tr } x_i = 1$. Hence starting from D real unconstrained optimization parameters, we have eliminated $1+m+2n(2n+1)$ real degrees of freedom to satisfy all required constraints on c and x_i , yielding the original number of D' real degrees of freedom.

Now we can directly compute the Lagrangian for each pair x_i, x_j via (2.5) and obtain the causal action by a weighted sum over these terms with weights $c_i c_j$. The eigenvalue computation of the products $x_i x_j$ can be computationally expensive, which

is why for $n = 1$ we instead compute the Lagrangian equivalently via the formula (see (5.7) and (5.8))

$$\mathcal{L}^{(n=1)}(x_i, x_j) := \frac{1}{2} \max \{0, 2 \operatorname{tr}((x_i x_j)^2) - \operatorname{tr}(x_i x_j)^2\} .$$

To conclude, setting $\Lambda := (\tilde{c}, \mu^+, \mu^-, B^1, B^2)$ for the collection of all optimization parameters, we can reformulate the constrained optimization problem (6.1) as the unconstrained optimization problem

$$\text{minimize } \mathcal{S}(\Lambda) \text{ over } \mathbb{R}^D ,$$

where we independently vary the real and imaginary parts of B^1, B^2 . Once we have implemented the causal action as a function of these D real parameters, automatic differentiation will provide us with a function that computes the gradient of the causal action at any input. Hence, provided an initial starting point, we can directly employ local, gradient-based optimization such as (L)-BFGS.

6.3. Initialization. Assuming no prior knowledge about the minimizer that we could encode directly into parameter values, we start with random initial parameter values from the following distributions. We draw the parameters \tilde{c} (from which we derive the weights c) independently from a normal distribution with mean 1 and small standard deviation σ_c to break potential symmetries. For the spectra, we allow to select an initial guess $\mu_0 > 0$ that may be motivated from analytical findings and draw the parameters μ^+ (and μ^-) independently from a normal distribution with mean $\log(\mu_0 + 1/n)$ (and $\log(\mu_0)$) and standard deviation σ_μ . Finally, we independently sample real and imaginary parts of all entries of B_i^1, B_i^2 uniformly from $(-\pi, \pi)$. We report details on the parameters $\sigma_c, \mu_0, \sigma_\mu$ as well as other parameters such as tolerances in (L)-BFGS for the different experiments in Appendix A.

7. THE ASYMPTOTICS FOR FIXED m AND LARGE f

7.1. Analytic Results. In this section we numerically investigate an asymptotic behavior that is analytically well understood and can serve as a first benchmark for our numerical approach. To this end, we fix the number m of spacetime points and let the Hilbert space dimension f grow large. In this limit, the causal action can be bounded from below as follows.

Proposition 7.1. *Assume that*

$$f \geq mn . \tag{7.1}$$

Then the minimum the causal action (2.6) is bounded below by

$$\mathcal{S}(\rho) \geq \mathcal{S}_{\min} := \frac{1}{2mn^3} . \tag{7.2}$$

The lower bound is attained by a weighted counting measure.

Proof. A weighted counting measure that attains the bound can be constructed as follows: Choose all operators x_i in the support of the measure so as to have the non-trivial eigenvalues (counting multiplicities)

$$\nu_1 = \dots \nu_n = \frac{1}{n} \quad \text{and} \quad \nu_{n+1} \dots \nu_{2n} = 0 .$$

Thus the image of each operator is only n -dimensional, and under the assumption (7.1) the operators x_1, \dots, x_m can then be chosen to have pairwise orthogonal images.

Then $\mathcal{L}(x_i, x_j)$ vanishes unless $i = j$. The eigenvalues of the operator product x^2 are $1/n^2$ and zero. Therefore,

$$\mathcal{L}(x_i, x_i) = \frac{1}{4n} 2 \sum_{i=1}^n \sum_{j=n+1}^{2n} \nu_i^4 = \frac{1}{2n} \frac{n^2}{n^4} = \frac{1}{2n^3}.$$

We next choose all the weights equal to $c_i = 1/m$. We thus obtain

$$\mathcal{S}(\rho) = \frac{1}{m^2} \sum_{i=1}^m \mathcal{L}(x_i, x_i) = \frac{1}{2n^3 m},$$

showing that the value \mathcal{S}_{\min} in (7.2) is attained.

In order to show that this value of the causal action is minimal, we slightly improve the estimate in [10, Proposition 4.3]: We denote the non-trivial eigenvalues of x by ν_1, \dots, ν_{2n} and order them such that

$$\nu_1, \dots, \nu_n \geq 0 \quad \text{and} \quad \nu_{n+1}, \dots, \nu_{2n} \leq 0.$$

Then, omitting the summands in (2.5) for which both $i, j \leq n$ or both $i, j > n$, we obtain

$$\mathcal{L}(x, x) \geq \frac{1}{4n} 2 \sum_{i=1}^n \sum_{j=n+1}^{2n} (\nu_i^2 - \nu_j^2)^2 = \frac{1}{2n} \sum_{i=1}^n \sum_{j=n+1}^{2n} (\nu_i - \nu_j)^2 (\nu_i + \nu_j)^2.$$

In this formula, the eigenvalues ν_i and ν_j have opposite sign. This gives the estimate

$$\mathcal{L}(x, x) \geq \frac{1}{2n} \sum_{i=1}^n \sum_{j=n+1}^{2n} (\nu_i + \nu_j)^4. \quad (7.3)$$

On the other hand, the trace of x can be estimated with the help of the Hölder inequality by

$$n = n \operatorname{tr} x = \sum_{i=1}^n \sum_{j=n+1}^{2n} (\nu_i + \nu_j) \leq \left(\sum_{i=1}^n \sum_{j=n+1}^{2n} (\nu_i + \nu_j)^4 \right)^{\frac{1}{4}} (n^2)^{\frac{3}{4}}.$$

Using this inequality in (7.3), we obtain the lower bound

$$\mathcal{L}(x, x) \geq \frac{1}{2n^3}.$$

This makes it possible to estimate the causal action by

$$\mathcal{S}(\rho) \geq \sum_{i=1}^m c_i^2 \mathcal{L}(x_i, x_i) \geq \frac{1}{2n^3} \sum_{i=1}^m c_i^2.$$

Using the Cauchy-Schwarz inequality

$$1 = \sum_{i=1}^m c_i \leq \left(\sum_{i=1}^m c_i^2 \right)^{\frac{1}{2}} \sqrt{m},$$

we obtain the desired lower bound in (7.2). \square

Specializing this result to the cases $n = 1$ and $n = 2$, we find that for

$$\begin{aligned} \text{large } f \text{ at } n = 1: & \quad \min \mathcal{S} \xrightarrow{f \rightarrow \infty} \frac{1}{2m} \\ \text{large } f \text{ at } n = 2: & \quad \min \mathcal{S} \xrightarrow{f \rightarrow \infty} \frac{1}{16m}. \end{aligned}$$

Having established this optimal lower bound for the causal action in the limit $f \rightarrow \infty$, we now state another lower bound for a specific class of measures in spin dimension $n = 1$.

Lemma 7.2. *Let $\rho = \sum_{i=1}^m \frac{1}{m} \delta_{x_i}$ be a normalized equal-weighted counting measure on \mathcal{F} in spin dimension $n = 1$ for which all operators x_i have rank one. Then*

$$\mathcal{S}(\rho) \geq \frac{1}{f(f+1)}. \quad (7.4)$$

Proof. Since the operators x_i have rank one and $\text{tr } x_i = 1$, all the x_i are projection operators to one-dimensional subspaces in \mathcal{H} , i.e., in bra/ket notation,

$$x_i = |v_i\rangle\langle v_i| \quad \text{with unit vectors } v_i \in \mathcal{H}.$$

As a consequence, the product of two operators $x_i x_j$ has rank at most one, and its non-trivial eigenvalue is given by $|\langle v_i | v_j \rangle|^2$. Hence

$$\mathcal{L}(x_i, x_j) = \frac{|\langle v_i | v_j \rangle|^4}{2}.$$

The (second) Welch bound [34] gives the estimate

$$\sum_{i,j=1}^m |\langle v_i | v_j \rangle|^4 \geq \frac{m^2}{\binom{f+1}{2}} = \frac{2m^2}{f(f+1)}.$$

We thus obtain the lower bound

$$\mathcal{S}(\rho) = \sum_{i,j} c_i c_j \mathcal{L}(x_i, x_j) = \frac{1}{2m^2} \sum_{i,j} \mathcal{L}(x_i, x_j) \geq \frac{1}{f(f+1)}.$$

This concludes the proof. \square

We point out that the last estimate applies only if all the operators have rank one. At least for very large m , this is not the case for minimizing measures, as the following argument shows. We choose k such that $2k \leq f \leq 2k+1$. Then we can construct k copies of a discrete Dirac sphere on k pairwise orthogonal, two-dimensional subspaces of \mathcal{H} . Then, in the limit $m \rightarrow \infty$, the causal action tends to

$$\mathcal{S} \rightarrow \frac{1}{k^2} \frac{\sqrt{3}}{4\pi}.$$

If f is even, we conclude that $\mathcal{S} \rightarrow \sqrt{3}/(\pi f^2)$, which is smaller than the lower bound in (7.4). Likewise, if f is odd, we obtain $\mathcal{S} \rightarrow \sqrt{3}/(\pi(f-1)^2)$, which is again smaller than the lower bound in (7.4) if $f \geq 7$.

This consideration shows that the assumptions of Lemma 7.2 are not satisfied asymptotically as $m \rightarrow \infty$. Nevertheless, the lower bound (7.4) will be helpful for interpreting our numerical results in the case $m > f$, as we will see in the next section.

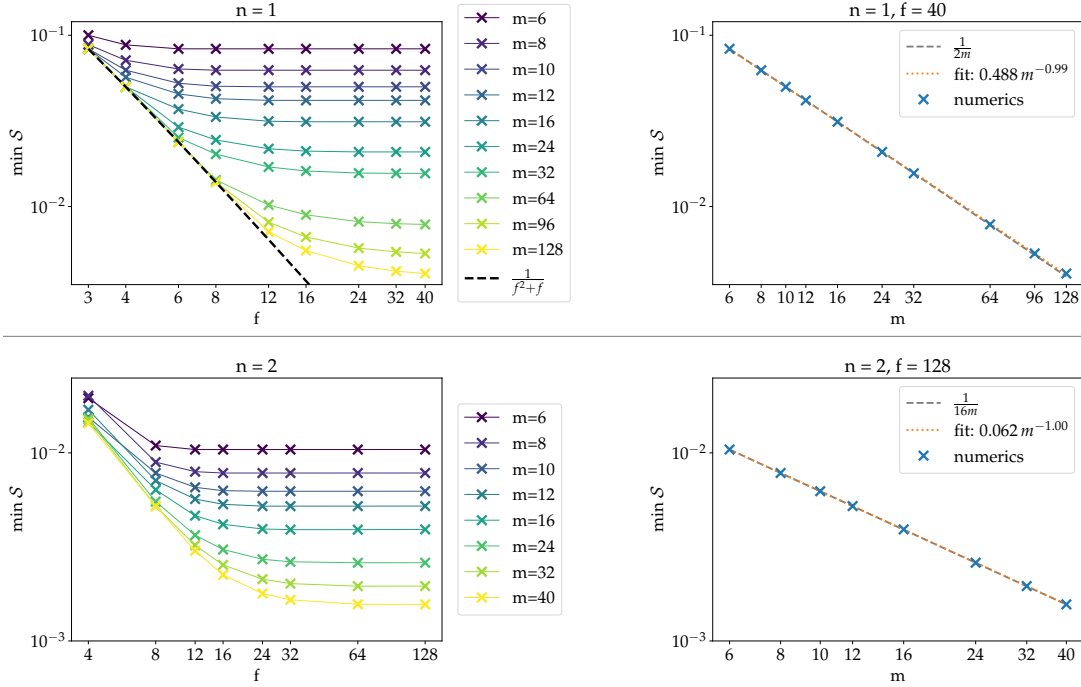


FIGURE 3. In the left column we show the numerically found minimal causal action for increasing values of f and m at $n = 1$ (top) and $n = 2$ (bottom). The right column then displays the scaling behavior of the minimal causal action at the largest value of f for each m . A simple linear least squares fit (in log-log space) confirms the analytic asymptotic behavior of \mathcal{S} as f becomes large for both $n = 1$ and $n = 2$.

7.2. Numerical Findings. Figure 3 shows that our numerical results reproduce the analytic asymptotics to great accuracy. We take this as first evidence that the numerical optimization scheme appears to find these simple minimizing configurations for various combinations of values of m and f , even for $D = 41$ 160-dimensional optimization problems. All these results were found from a single random starting point.

Whereas this section focuses on the large f limit, the upper row in Figure 3 for spin dimension $n = 1$ also shows data for $m > f$. Here we see that the numerically found configurations only exceed the $\mathcal{S} \propto 1/(2m)$ scaling of the causal action by very small values, despite the violation of the assumption of Proposition 7.1. This is not surprising in view of Lemma 7.2, which shows that the value $\mathcal{S}(\rho) = 1/(f^2 + f)$ can be achieved if there exists a choice of m unit vectors in \mathbb{C}^f attaining equality in the relevant Welch bound. In fact, the upper left plot in Figure 3 shows that for $m > f$, the numerically found configurations follow this asymptotic behavior. We also find for these numerical configurations that all spacetime point operators are (within the numerical accuracy) projection operators of rank one. Nevertheless, as discussed after Lemma 7.2, the causal action can be lowered below $\mathcal{S} = 1/(f^2 + f)$ for sufficiently large m . We do not see this effect in our numerics, however, probably because the considered values of m are not large enough.

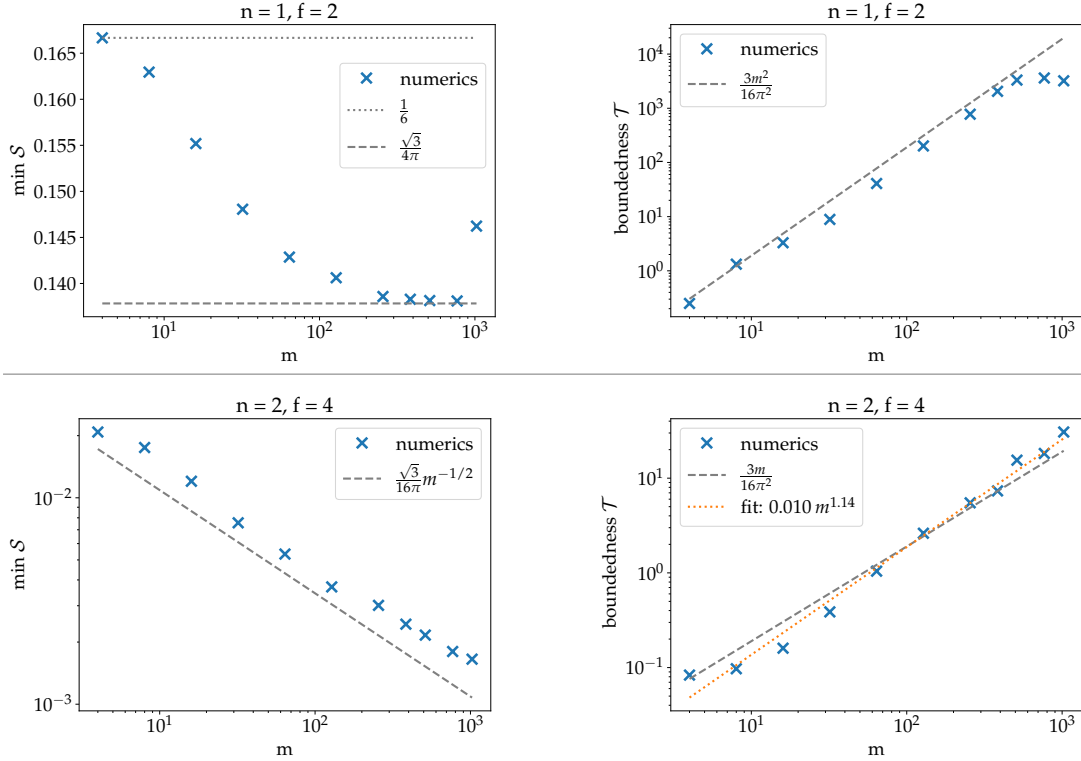


FIGURE 4. The minimal causal action (left) and value of the boundedness functional (right) found numerically for $n = 1, f = 2$ (top row) and $n = 2, f = 4$ (bottom row) as m increases.

8. NUMERICAL STUDY OF DISCRETE DIRAC SPHERES

In this section we study the asymptotic behavior of the causal action when the Hilbert space dimension is kept minimal at $f = 2n$ but the number m of spacetime points grows. In both cases $n = 1$ and $n = 2$, our results follow the asymptotic behavior expected from the analytical results on discrete Dirac spheres from Sections 3.4 and 4. The numerically found causal actions come close but do not get below the values calculated there.

For the numerical results of this section, each individual optimization was repeated for ten different random starting points, and results are reported only for the run with the smallest final value of \mathcal{S} .

8.1. Spin Dimension One. In the case $f = 2$, Proposition 3.3 shows that for the two-dimensional discrete Dirac sphere the causal action approaches $\mathcal{S} \rightarrow \frac{\sqrt{3}}{4\pi}$ as $m \rightarrow \infty$ for $\tau \propto \sqrt{m}$, and (3.17) in Proposition 3.2 shows that for an isotropic distribution of spacetime points at fixed $\tau = 1$ the causal action approaches $\mathcal{S} \rightarrow \frac{1}{6}$ as $m \rightarrow \infty$. The top row in Figure 4 shows the results of our numerical optimization. As m increases, the minimal causal action indeed drops from the upper bound at $\frac{1}{6}$ for small m to the analytical minimum of Proposition 3.3 for $m \approx 1000$. We note that for large m the dimensionality of the optimization problem is of the order of 10^4 , and we stopped

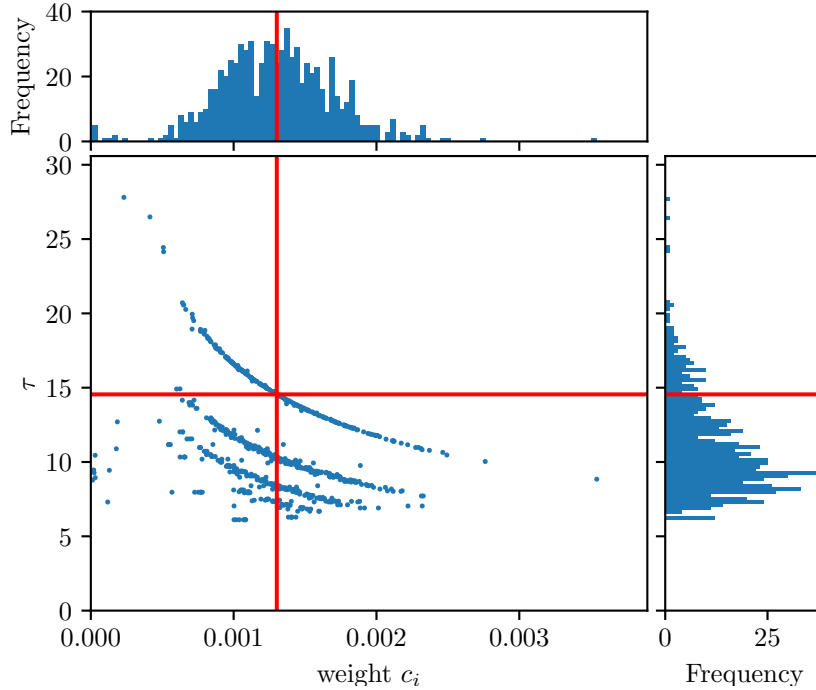


FIGURE 5. Clustering in the numerical configuration for $n = 1, f = 2, m = 768$. Red lines indicate expectations from discrete Dirac sphere.

all optimization runs after 3 days, which is why runs for $m = 1024$ have not fully converged.

The right plot in the top row of Figure 4 shows that the asymptotic growth rate of the boundedness functional at first is quadratic for large m and closely matches the analytic results from Proposition 3.4, i.e., $\mathcal{T} = \frac{3}{16\pi^2}m^2 + \mathcal{O}(m)$. However, for the largest values of m , it deviates from the expected scaling. This can be explained by the fact, that in the numerical configurations the values of τ_i have a certain spread where most τ_i may even lie significantly below the value expected from the discrete Dirac sphere. This is shown in Figure 5.

This figure also reveals another surprising feature of the numerically found configurations. When plotting τ_i versus the weight c_i of the spacetime points of a numerical minimizer, one sees that the points tend to accumulate on several hyperbolas with

$$\tau_i^2 c_i = \text{const.}$$

The first, upper-most of these hyperbolas goes through the point (τ, c) corresponding to the parameter values of the discrete Dirac sphere (see the red cross hair in the figure) in Section 3.4. In fact, the spacetime points belonging to this hyperbola are (essentially) all pairwise spacelike separated from each other. Hence, they can be understood as a discrete Dirac sphere configuration which is causally trivial (as defined and analyzed in Section 3.5), in which the τ_i vary and the weights c_i are adjusted according to (3.27). The spacetime points on the other hyperbolas, however, are not causally trivial. Instead, on the first hyperbola below the causally trivial hyperbola, every

spacetime point is timelike separated to itself and to one other spacetime point. Similarly, on the second hyperbola every spacetime point has two partners with timelike separation. Generally speaking, the spacetime points form groups with timelike separation within each group but spacelike separation between points in different groups. The points within each group are in a quite simple configuration: they have almost the same value of τ , have almost the same weight, and the corresponding vectors \vec{x} in the representation (3.2) are very close to each other. Therefore, each group can be viewed as a “cluster” of nearby points on \mathcal{F} with equal weight factors. If one replaces each cluster by a single point (with the weight taken as the sum of the weights of the cluster points), then the resulting spacetime point lies again on the uppermost, causally trivial hyperbola in Figure 5. In this way, we obtain a numerical configuration which coincides with a discrete Dirac sphere configuration, except that the values of τ are smeared out. Keeping in mind that the numerical values of the causal action always lie slightly above the value for the discrete Dirac sphere, our findings support the conjecture that the absolute minimizers for large m should indeed be discrete Dirac sphere configurations. We expect that the numerical configurations with more spread out values of τ correspond to local minima.

8.2. Spin Dimension Two. For $f = 4$, Proposition 4.2 shows that for the four-dimensional Dirac sphere $\mathcal{S} = \frac{\sqrt{3}}{16\pi\sqrt{m}} + \mathcal{O}(m^{-\frac{3}{2}})$ for $\tau \propto m^{\frac{1}{4}}$. The bottom row in Figure 4 shows the results of our numerical optimization. While the found configurations do not reproduce the analytical values for the minimal causal action precisely, they are reasonably close and—more importantly—reproduce the correct scaling behavior. We remark once again that these are non-convex, non-smooth optimization problems in high dimensions ($D = 37888$ for $m = 1024$) tackled with local quasi-Newton methods. The analytic asymptotic scaling behavior of the boundedness functional for large m from Proposition 4.3 in leading order becomes $\mathcal{T} = \frac{3}{16\pi^2} m$ when substituting τ from (4.7). This value is reproduced by our numerics with good accuracy.

To summarize, the numerics presented in this section yield strong evidence for the conjecture that minimizers of the causal action principle for large m are close to the two- and four-dimensional discrete Dirac spheres, respectively.

9. NUMERICAL STUDY BEYOND DISCRETE DIRAC SPHERES

At present, it is an open problem to understand the asymptotic behavior of the causal action for a large number m of spacetime points for fixed Hilbert space dimension f . In the previous sections, we found that our numerical results support our analytic understanding and confirm conjectures on the behavior of minimizers in the minimal Hilbert space dimension $f = 2n$ (again for large m). However, beyond this case of minimal Hilbert space dimension, no analytic candidates for asymptotic minimizers are known. Therefore, it is an important task to use our numerical methods in order to explore and understand these cases better.

In the case of spin dimension $n = 2$, already in the minimal case $f = 4$ we showed that the causal action tends to zero as for large m at least at the rate $\mathcal{S} \propto \frac{1}{\sqrt{m}}$. Since the infimum of the causal action is monotone decreasing in f , the causal action also tends to zero for if $f > 4$, but the rate of decay in m could be faster. In the case of spin dimension $n = 1$, the situation is even less clear, because it is not known if there are measures that achieve arbitrary low values of the causal action as $m \rightarrow \infty$, or if,

conversely, for each fixed f there exists a strictly positive lower bound of the causal action.

In the case $f = 2$, the numerical results seem to support the conjectures that all minimizers for large m are close to the two-dimensional (3.24) provides a universal lower bound for the causal action. However, already in the case $n = 1, f = 3$ no analytic candidate for a minimizer is known asymptotically for large m . The basic difficulty can be understood as follows. In the case $n = 1, f = 2$, the set \mathcal{F} can be parametrized by linear combinations of the identity matrix and the three Pauli matrices (see (3.2)). Here a natural candidate for minimizers is the discrete Dirac sphere (see Section 3.4). The fact that the anti-commutation relations of the Pauli matrices play a special role in the computation of the causal Lagrangian motivates higher-dimensional discrete Dirac spheres, like the four-dimensional discrete Dirac sphere introduced in Section 4. Such discrete Dirac sphere configurations exist only for specific choices of f and n . This follows from the representation theory of Clifford algebras (for details see for example [23] or [32]). More specifically, f must be the dimension of an irreducible Euclidean Clifford representation, giving rise to the

$$2k\text{-dimensional discrete Dirac sphere for } n = 2^{k-1} \text{ and } f = 2^k$$

with $k \in \mathbb{N}$. Since there is no irreducible Clifford representation on \mathbb{C}^3 , in the case $f = 3$ there is no discrete Dirac sphere.

In view of this lack of analytic candidates, the numerical investigation of the case $n = 1$ and $f = 3$ can serve the important task of building intuition and gaining a better understanding of the structure of minimizers. To this end, it is helpful to represent the numerically found discrete spacetime in a way which gives insight into its geometric and causal structure. This is accomplished by the *projected spacetime plot*, which visualizes the spacetime as seen from a chosen reference point, based on the geometric cone structures uncovered in Section 5.

The projected spacetime plot is obtained as follows. We let $(c_i, x_i)_{i=1, \dots, m}$ with $c_i \geq 0$ and $x_i \in \mathcal{F}$ be a numerical minimizer. We choose one point (c_j, x_j) with $j \in \{1, \dots, m\}$ as our reference point. For consistency with the notation in Section 5, we denote this reference point by $x = x_j$. Then the image of the spacetime point operator $x(\mathcal{H})$ is a two-dimensional subspace of \mathcal{H} (this subspace is the so-called spin space of the spacetime point; for details see for example [12, Section 1.1] or [16, Section 5.6]). For convenience, we work in an eigenvector basis of $x(\mathcal{H})$, where our reference point has the matrix representation (5.2). Next, we let $y = x_i$ be any spacetime point. Using that the Lagrangian $\mathcal{L}(x, y)$ can be computed from the operator product $x \pi_x y \pi_x$, we consider, instead of y , the projection $\pi_x y \pi_x$ of y to $x(\mathcal{H})$ and represent it according to (5.3) in terms of real coordinates (y_0, \dots, y_3) . We want to plot these coordinates for all spacetime points x_1, \dots, x_m in such a way that the causal structures as well as the distances between these points become visible. In view of (5.6), plotting the coordinates

$$\hat{y}_0 := y_3 + y_0 \tau \quad \text{and} \quad \hat{y}_{1/2} := \sqrt{\tau^2 - 1} y_{1/2},$$

the causal relations between the reference point x and the spacetime point y coincide with that of three-dimensional Minkowski space $\mathbb{R}^{1,2}$ with the metric

$$\langle (\hat{y}_0, \hat{y}_1, \hat{y}_2), (\hat{y}_0, \hat{y}_1, \hat{y}_2) \rangle_{\mathbb{R}^{1,2}} := \hat{y}_0^2 - \hat{y}_1^2 - \hat{y}_2^2.$$

In order to simplify the plot, we make use of the fact that the causal Lagrangian $\mathcal{L}(x, y)$ is rotationally symmetric in the $\hat{y}_1 - \hat{y}_2$ -plane. This is also reflected by our numerical

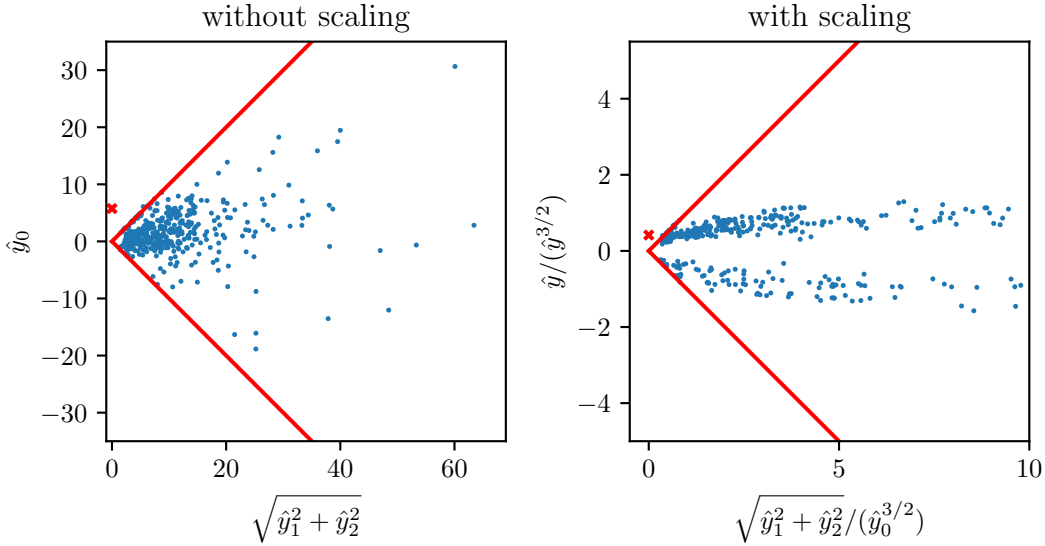


FIGURE 6. Projected spacetime plot, without and with the scaling (9.1), for a numerical configuration with $n = 1, f = 3, m = 512$. The red lines indicate the causal cone of the reference point, whose position inside the cone is marked by a cross.

minimizers which do seem to distinguish a direction in this plane. Therefore, it is preferable to plot \hat{y}_3 versus $\sqrt{\hat{y}_1^2 + \hat{y}_2^2}$, as shown on the left of Figure 6.

In order to get the correct intuition about distances, one should keep in mind that the projections π_x make the parameters (y_0, \dots, y_3) smaller for points which are to be thought of as being further apart from x . More specifically, one can argue as follows. If the parameters (y_0, \dots, y_3) are large and the points x and y are timelike separated, then the Lagrangian $\mathcal{L}(x, y)$ is typically large. In concrete examples, the Lagrangian decays if the spacetime points are far apart. Therefore, points for large $\mathcal{L}(x, y)$ should correspond to points which are close together.

This picture becomes more precise with the following scaling argument. Having two spatial dimensions in mind, Dirac wave functions have the length dimension minus one (because $\int_{\mathbb{R}^2} |\psi| d^2x$ is a dimensionless probability). Since the local correlation operators involve two wave functions, they have the length dimension minus two. Therefore, in order to obtain Minkowski vectors with the dimension of length, one should plot the vectors

$$\frac{1}{|\hat{y}_0|^{\frac{3}{2}}} (\hat{y}_0, \hat{y}_1, \hat{y}_2). \quad (9.1)$$

This gives plots as shown on the right of Figure 6.

In this way, the causal fermion system can be visualized by a discrete subset of Minkowski space. The causal structure of Minkowski space coincides with the causal relations between the reference point x and all the other spacetime points. Moreover, the size of the Minkowski vector gives an indication of the “distance” between x and y .

The numerical data obtained for $n = 1, f = 3$ for spacetime point numbers up to $m = 768$, obtained within the scope of this work, do not yield conclusive results

for a potential lower bound of the causal action. To this end, it appears necessary to increase m by at least one order of magnitude. This, in turn, makes it necessary to improve the efficiency of our numerical approach.

10. CONCLUSION AND OUTLOOK

The main conclusion of the present work is to demonstrate that differentiable programming methods give a major advance in the numerical study of the causal action principle for causal fermion systems. We gave a detailed analysis in the cases $n = 1, f = 2$, $n = 1, f = 3$ and $n = 2, f = 4$. In the cases $n = 1, f = 2$ and $n = 2, f = 4$, our results support the conjecture that, asymptotically for large m , the absolute minimizers should be close to discrete Dirac sphere configurations.

Our analysis gave new insight into the structure of minimizing measures. In particular, for spin dimension $n = 1$, the causal relations could be formulated geometrically in terms of causal cones. Moreover, as a helpful tool to build intuition for the structure of numerically found minimizers, we introduced projected spacetime plots which visualize the causal and geometric structure of the resulting discrete spacetimes as seen from an arbitrary reference point.

We see several directions for future research. First, we plan to complement the numerical toolbox by linear programming methods in convex domains (in this case, one approximates \mathcal{F} by a sufficiently large discrete set and minimizes the causal action under the variation of the weights in the convex set $\{0 \leq c_i \text{ and } \sum_i c_i = 1\}$). Another open problem concerns the asymptotics of the minimal causal action for fixed n and f and large m (except for the cases $n = 1, f = 2$ and $n = 2, f = 4$, which are already well-understood). Finally, the major goal of future research will be to analyze the case of larger f numerically. This is a challenging problem, because the number of degrees of freedom grows linearly in f . Therefore, an efficient numerical study requires more sophisticated methods which are more adapted to the structure of a causal action principle. We plan to develop these methods in the near future.

Acknowledgments: R.H.J. gratefully acknowledges support by the Wenner-Gren Foundations.

APPENDIX A. DETAILS OF THE IMPLEMENTATION

All our code is implemented in Python 3.9 [33] making use of JAX [7], Numpy [21], Scipy [21], Matplotlib [22] for visualizations, as well as abseil-py² and tqdm³.

Throughout all our experiments we fix the parameters $\sigma_c = \sigma_\mu = 0.01$ and choose μ_0 as a function of m following Proposition 3.3

$$\mu_0^{(n=1)}(m) = \frac{5}{4} \left(3^{\frac{1}{4}} \sqrt{\frac{m}{2\pi}} - 1 \right)$$

for all experiments with $n = 1$ and following Proposition 4.2

$$\mu_0^{(n=2)}(m) = \frac{1}{4} \left(\frac{(3m)^{\frac{1}{4}}}{\sqrt{\pi}} - 1 \right)$$

for $n = 2$.

²<https://github.com/abseil/abseil-py>

³<https://github.com/tqdm/tqdm>

We use the Scipy implementations of (L)-BFGS. We start the optimization with L-BFGS and parameters $\text{ftol} = 10^{-7}$, $\text{gtol} = 10^{-9}$ keeping 70 terms to approximate the Hessian (for limited memory) and using at most 20 line search steps in each iteration. Here ftol and gtol are tolerances used in the stopping criteria of the optimization. The optimization halts as soon as the absolute or relative change of the objective function between two iterations is smaller than ftol , or the ℓ_1 norm of the projected gradient is smaller than gtol , or the maximum number of 10,000 iterations has been reached. We then continue the optimization from the last point with full BFGS with $\text{gtol} = 10^{-7}$ for at most 5000 iterations.

A key advancement of our method is that (L)-BFGS does not rely on finite-difference approximations for gradients, but the gradient function can be automatically computed via differential programming. To this end, we use the JAX package [7], which does not only allow for automatic differentiation, but also includes hardware-specific just-in-time compilation (jit) of Python functions to vastly speed up computations. We now provide a summary of the overall structure of our implementation in Python syntax. The full implementation including the found minimizers is publicly available at <https://github.com/nikikilbertus/causal-fermion-systems>.

```

1 import jax # popular differentiable programming framework
2 from scipy.optimize import minimize
3
4 # A function to initialize the D real optimization parameters
5 def initialize_parameters():
6     ...
7     return parameters
8
9 # The causal action as a function of the optimization parameters
10 def action(parameters):
11     ...
12     return action
13
14 # Automatically get the gradient function for the action
15 gradient = jax.grad(action)
16
17 # Hardware specific just-in-time compilation for speed-up
18 fast_action = jax.jit(action)
19 fast_gradient = jax.jit(gradient)
20
21 # Initialize the D optimization parameters (randomly)
22 initial_parameters = initialize_parameters()
23
24 # Assume a BFGS implementation is available requiring
25 # the objective, gradient, and initial guess
26 minimal_parameters = minimize(
27     fun=fast_action, # objective function
28     x0=initial_parameters, # initial guess
29     method="BFGS", # or "L-BFGS-B"
30     jac=fast_gradient, # gradient function
31     options={...} # parameters for stopping criteria
32 )

```

```

33 # 'minimal_parameters' is a data structure containing the
34 # minimal parameter vector as the field 'x' alongside
35 # information about convergence
36
37 # Compute the action for the minimizer
38 minimal_action = action(minimal_paramters.x)

```

LISTING 1. Structure of the optimization procedure in Python.

REFERENCES

- [1] *Link to web platform on causal fermion systems: www.causal-fermion-system.com.*
- [2] A. Asl and M.L. Overton, *Analysis of limited-memory bfgs on a class of nonsmooth convex functions*, IMA Journal of Numerical Analysis **41** (2021), no. 1, 1–27.
- [3] L. Bäuml, F. Finster, H. von der Mosel, and D. Schiefeneder, *Singular support of minimizers of the causal variational principle on the sphere*, arXiv:1808.09754 [math.CA], Calc. Var. Partial Differential Equations **58** (2019), no. 6, 205.
- [4] A.G. Baydin, B.A. Pearlmutter, A.A. Radul, and J.M. Siskind, *Automatic differentiation in machine learning: a survey*, arXiv:1502.05767 [cs.SC], Journal of machine learning research **18** (2018).
- [5] J. Bierler, *Numerische Untersuchung kausaler Variationsprinzipien*, Masterarbeit Mathematik, Universität Regensburg (2019).
- [6] J.D. Bjorken and S.D. Drell, *Relativistic Quantum Mechanics*, McGraw-Hill Book Co., New York, 1964.
- [7] J. Bradbury, R. Frostig, P. Hawkins, M.J. Johnson, C. Leary, D. Maclaurin, G. Necula, A. Paszke, J. VanderPlas, S. Wanderman-Milne, and Q. Zhang, *JAX: composable transformations of Python+NumPy programs*, <http://github.com/google/jax>, version 0.2.5 (2018).
- [8] J.H. Conway and N.J.A. Sloane, *Sphere Packings, Lattices and Groups*, third ed., Grundlehren der Mathematischen Wissenschaften [Fundamental Principles of Mathematical Sciences], vol. 290, 1999.
- [9] A. Diethert, F. Finster, and D. Schiefeneder, *Fermion systems in discrete space-time exemplifying the spontaneous generation of a causal structure*, arXiv:0710.4420 [math-ph], Int. J. Mod. Phys. A **23** (2008), no. 27/28, 4579–4620.
- [10] F. Finster, *A variational principle in discrete space-time: Existence of minimizers*, arXiv:math-ph/0503069, Calc. Var. Partial Differential Equations **29** (2007), no. 4, 431–453.
- [11] ———, *Causal variational principles on measure spaces*, arXiv:0811.2666 [math-ph], J. Reine Angew. Math. **646** (2010), 141–194.
- [12] ———, *The Continuum Limit of Causal Fermion Systems*, arXiv:1605.04742 [math-ph], Fundamental Theories of Physics, vol. 186, Springer, 2016.
- [13] ———, *Causal fermion systems: Discrete space-times, causation and finite propagation speed*, arXiv:1812.00238 [math-ph], J. Phys.: Conf. Ser. **1275** (2019), 012009.
- [14] F. Finster and M. Jokel, *Causal fermion systems: An elementary introduction to physical ideas and mathematical concepts*, arXiv:1908.08451 [math-ph], Progress and Visions in Quantum Theory in View of Gravity (F. Finster, D. Giulini, J. Kleiner, and J. Tolksdorf, eds.), Birkhäuser Verlag, Basel, 2020, pp. 63–92.
- [15] F. Finster and S. Kindermann, *A gauge fixing procedure for causal fermion systems*, arXiv:1908.08445 [math-ph], J. Math. Phys. **61** (2020), no. 8, 082301.
- [16] F. Finster, S. Kindermann, and J.-H. Treude, *An Introductory Course on Causal Fermion Systems*, in preparation, www.causal-fermion-system.com/intro-public.pdf.
- [17] F. Finster and J. Kleiner, *Causal fermion systems as a candidate for a unified physical theory*, arXiv:1502.03587 [math-ph], J. Phys.: Conf. Ser. **626** (2015), 012020.
- [18] ———, *A Hamiltonian formulation of causal variational principles*, arXiv:1612.07192 [math-ph], Calc. Var. Partial Differential Equations **56:73** (2017), no. 3, 33.
- [19] F. Finster and D. Schiefeneder, *On the support of minimizers of causal variational principles*, arXiv:1012.1589 [math-ph], Arch. Ration. Mech. Anal. **210** (2013), no. 2, 321–364.
- [20] J. Guo and A.S. Lewis, *Nonsmooth variants of Powell’s BFGS convergence theorem*, SIAM Journal on Optimization **28** (2018), no. 2, 1301–1311.

- [21] C.R. Harris, K.J. Millman, S.J. van der Walt, R. Gommers, P. Virtanen, D. Cournapeau, E. Wieser, J. Taylor, S. Berg, N.J. Smith, R. Kern, M. Picus, S. Hoyer, M.H. van Kerkwijk, M. Brett, A. Haldane, J. Fernández del Río, M. Wiebe, P. Peterson, P. Gérard-Marchant, K. Sheppard, T. Reddy, W. Weckesser, H. Abbasi, C. Gohlke, and T.E. Oliphant, *Array programming with NumPy*, Nature (2020).
- [22] J.D. Hunter, *Matplotlib: A 2D graphics environment*, Computing in Science & Engineering (2007).
- [23] H.B. Lawson, Jr. and M.-L. Michelsohn, *Spin Geometry*, Princeton Mathematical Series, vol. 38, Princeton University Press, Princeton, NJ, 1989.
- [24] A.S. Lewis and M.L. Overton, *Nonsmooth optimization via BFGS*, Submitted to SIAM J. Optimization (2009), 1–35.
- [25] ———, *Nonsmooth optimization via quasi-Newton methods*, Mathematical Programming **141** (2013), no. 1, 135–163.
- [26] J. Nocedal and S. Wright, *Numerical Optimization*, Springer Science & Business Media, 2006.
- [27] M.E. Peskin and D.V. Schroeder, *An Introduction to Quantum Field Theory*, Addison-Wesley Publishing Company Advanced Book Program, Reading, MA, 1995.
- [28] M.J.D. Powell, *Some global convergence properties of a variable metric algorithm for minimization without exact line searches*, Nonlinear programming, SIAM-AMS proceedings, vol. 9, 1976.
- [29] M. Reed and B. Simon, *Methods of Modern Mathematical Physics. IV, Analysis of operators*, Academic Press, New York, 1978.
- [30] E.B. Saff and A.B.J. Kuijlaars, *Distributing many points on a sphere*, Math. Intelligencer **19** (1997), no. 1, 5–11.
- [31] N.J.A. Sloane, *Tables of sphere packings and spherical codes*, IEEE Trans. Inform. Theory **27** (1981), no. 3, 327–338.
- [32] J. Snygg, *Clifford Algebra*, Oxford University Press, New York, 1997, A computational tool for physicists.
- [33] G. van Rossum and F.L. Drake, *Python 3 Reference Manual*, CreateSpace, 2009.
- [34] L. Welch, *Lower bounds on the maximum cross correlation of signals (Corresp.)*, IEEE Transactions on Information Theory **20** (1974), no. 3, 397–399, Conference Name: IEEE Transactions on Information Theory.

FAKULTÄT FÜR MATHEMATIK, UNIVERSITÄT REGENSBURG, D-93040 REGENSBURG, GERMANY
Email address: `finster@ur.de`

MAX PLANCK INSTITUTE OF QUANTUM OPTICS, HANS-KOPFERMANN-STR. 1, D-85748 GARCHING, GERMANY
Email address: `robert.jonsson@mpq.mpg.de`

DEPARTMENT OF INFORMATICS, TECHNICAL UNIVERSITY OF MUNICH, BOLTZMANNSTR. 3, D-85748 GARCHING, GERMANY

HELMHOLTZ AI, INGOLSTÄDTER LANDSTRASSE 1, D-85764 NEUHERBERG, GERMANY
Email address: `niki.kilbertus@tum.de`